

Determining the orientation of a magnetic reconnection X line and implications for a 2D coordinate system

Richard E. Denton¹, Yi-Hsin Liu¹, Jefferson A Agudelo Rueda¹, Kevin J Genestreti², Hiroshi Hasegawa³, Martin Hosner⁴, Roy B Torbert⁵, and James L Burch²

¹Dartmouth College

²Southwest Research Institute

³Institute of Space and Astronautical Science, JAXA

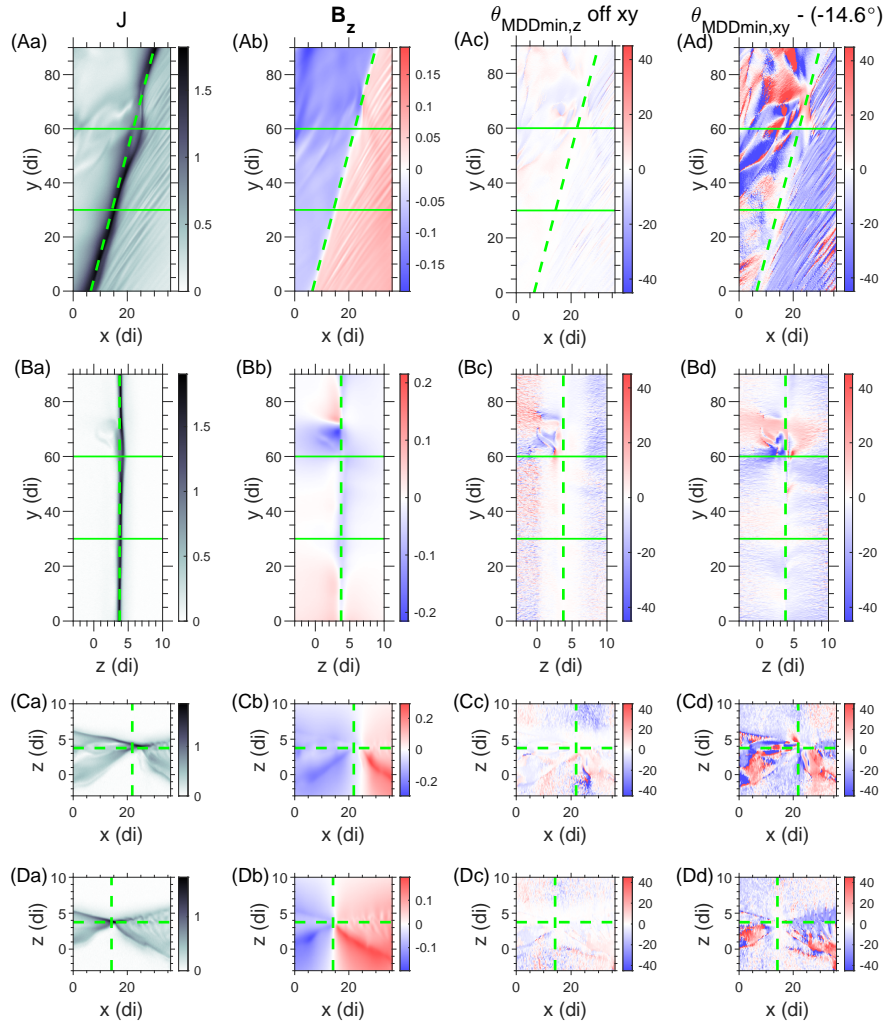
⁴Space Research Institute, Austrian Academy of Sciences

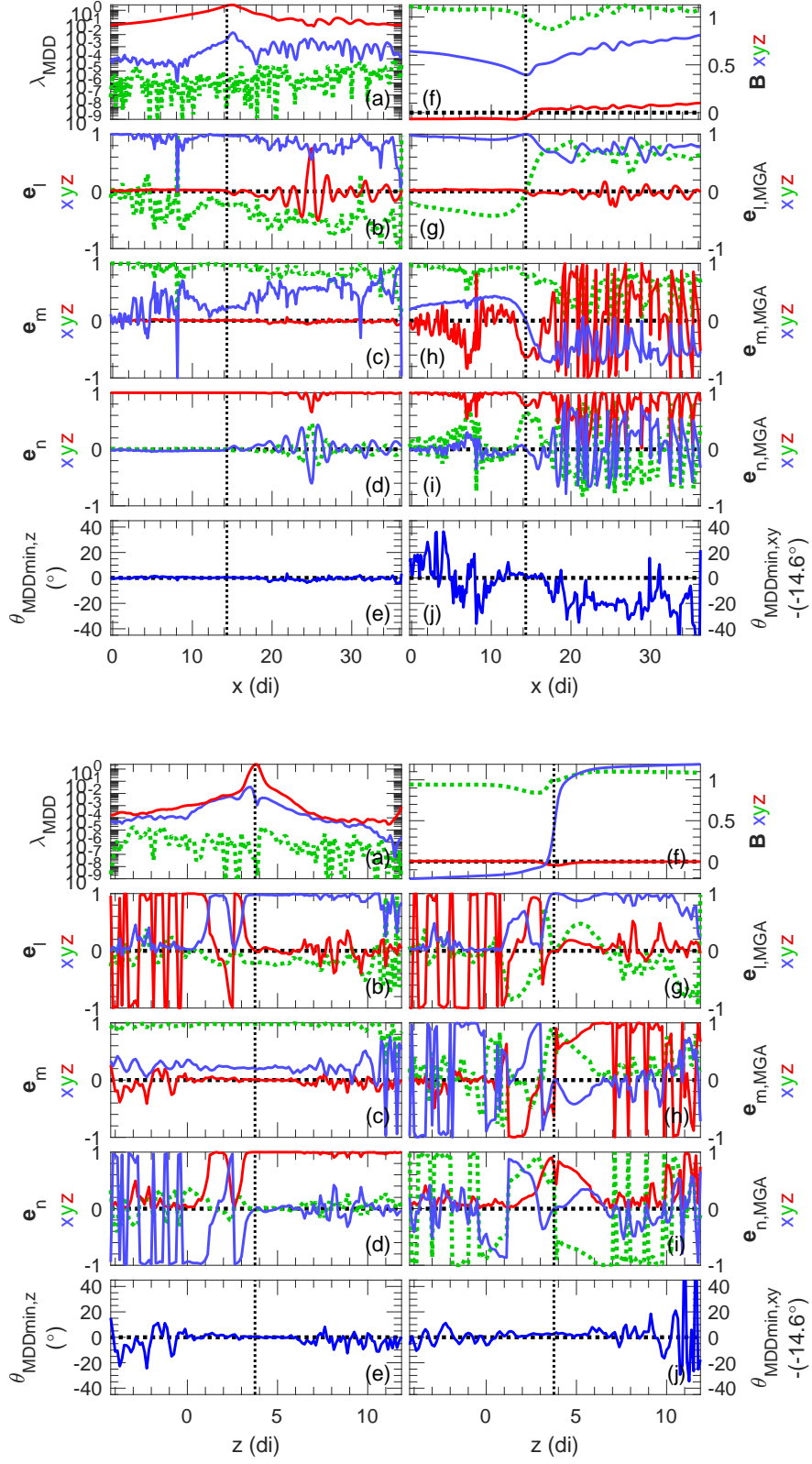
⁵University of New Hampshire

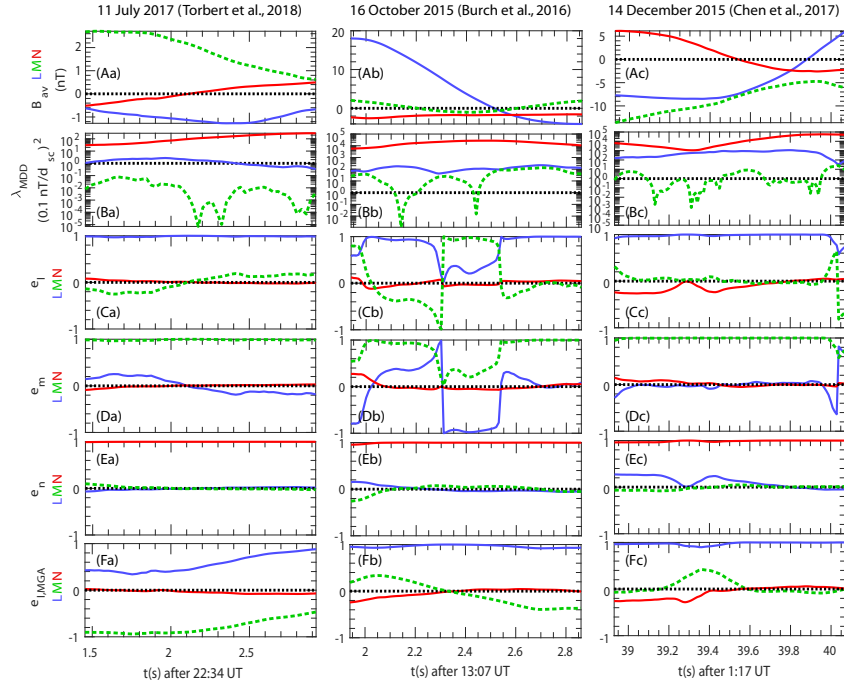
October 27, 2023

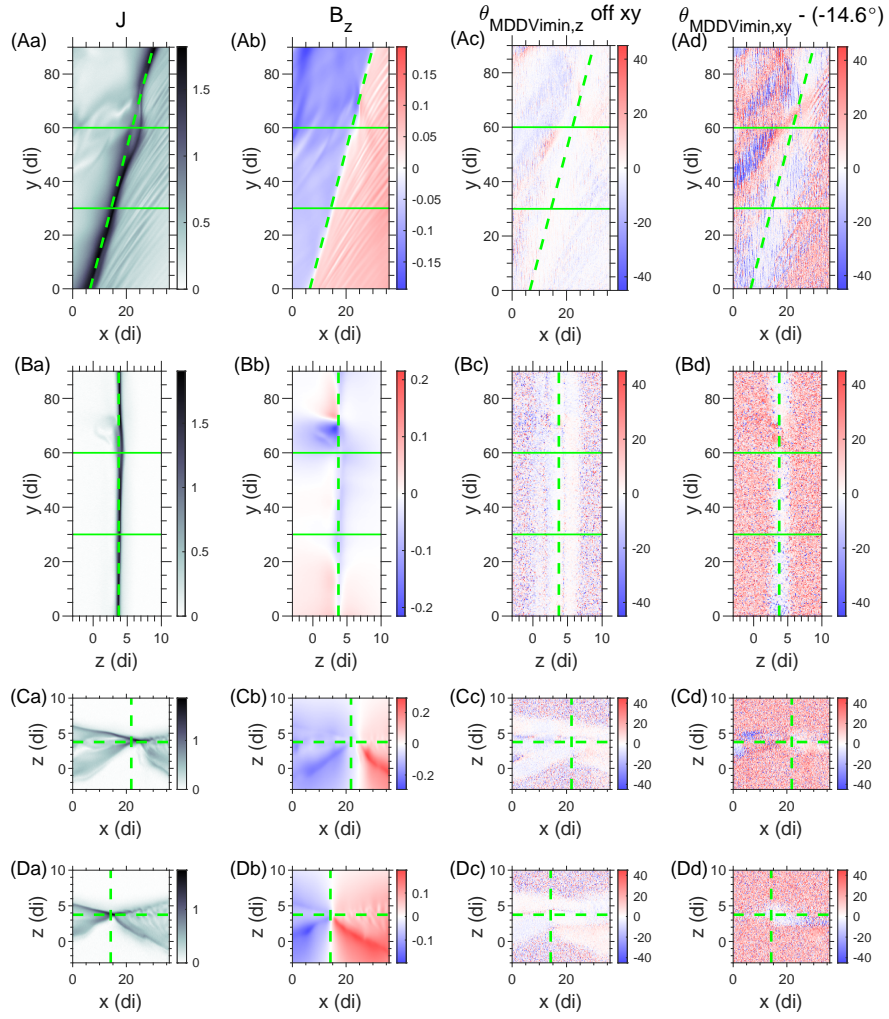
Abstract

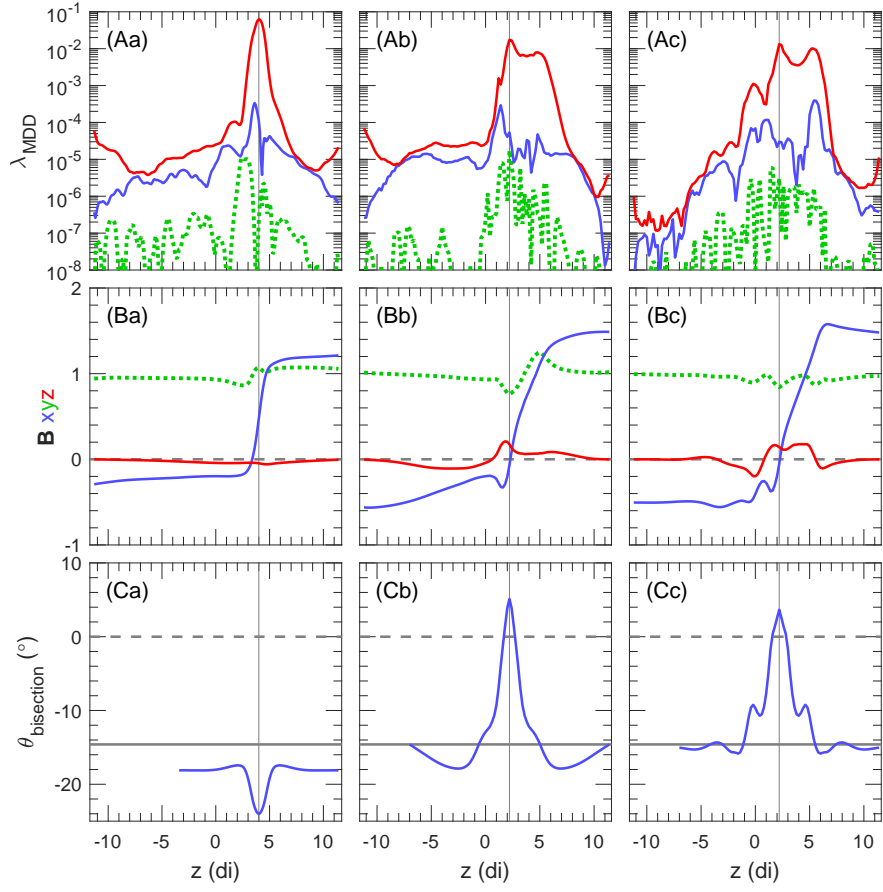
An LMN coordinate system for magnetic reconnection events is sometimes determined by defining N as the direction of the gradient across the current sheet and L as the direction of maximum variance of the magnetic field. The third direction, M , is often assumed to be the direction of zero gradient, and thus the orientation of the X line. But when there is a guide field, the X line direction may have a significant component in the L direction defined in this way. For a 2D description, a coordinate system describing such an event would preferably be defined using a different coordinate direction M' oriented along the X line. Here we use a 3D particle-in-cell simulation to show that the X line is oriented approximately along the direction bisecting the asymptotic magnetic field directions on the two sides of the current sheet. We describe two possible ways to determine the orientation of the X line from spacecraft data, one using the minimum gradient direction from Minimum Directional Derivative analysis at distances of the order of the current sheet thickness from the X line, and another using the bisection direction based on the asymptotic magnetic fields outside the current sheet. We discuss conditions for validity of these estimates, and we illustrate these conditions using several Magnetospheric Multiscale (MMS) events. We also show that intersection of a flux rope due to secondary reconnection with the primary X line can destroy invariance along the X line and negate the validity of a two-dimensional description.

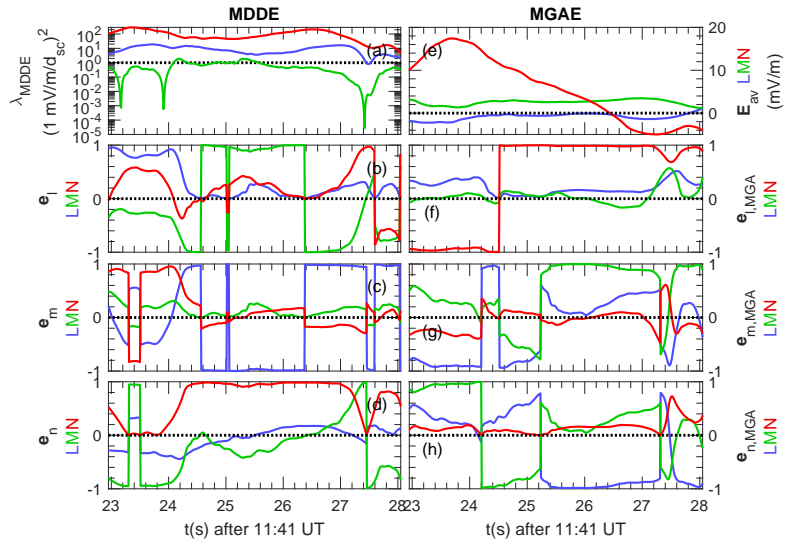


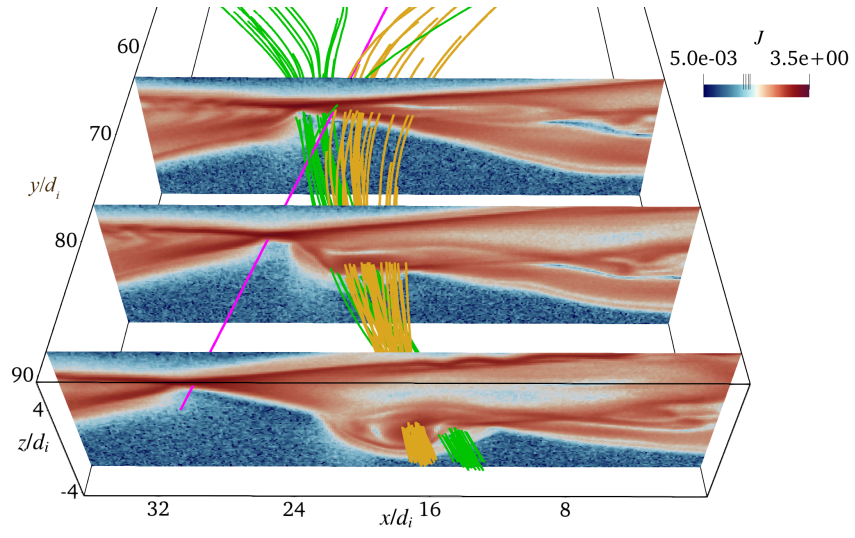












Determining the orientation of a magnetic reconnection X line and implications for a 2D coordinate system

Richard E. Denton¹, Yi-Hsin Liu¹, Jefferson A. Agudelo Rueda¹,
Kevin J. Genestreti², Hiroshi Hasegawa³, Martin Hosner^{4,5}, Roy B. Torbert⁶,
and James L. Burch⁷

¹Department of Physics and Astronomy, Dartmouth College, Hanover, New Hampshire, USA

²Space Science and Engineering Division, Southwest Research Institute, Durham, New Hampshire, USA

³Institute of Space and Astronautical Science, JAXA, Sagami-hara, Japan

⁴Space Research Institute, Austrian Academy of Sciences, 8042 Graz, Austria

⁵Institute of Physics, University of Graz, 8010 Graz, Austria

⁶Institute for the Study of Earth, Oceans, and Space, University of New Hampshire, Durham, New
Hampshire, USA

⁷Space Science and Engineering Division, Southwest Research Institute, San Antonio, Texas, USA.

Key Points:

- When there is a guide field, the orientation of the X line may be tilted toward the direction of maximum magnetic field variance
- Under certain circumstances Minimum Directional Derivative analysis can be used to determine the orientation of the X line
- Intersection of a flux rope with the primary X line due to secondary reconnection can destroy two dimensionality

Abstract

An LMN coordinate system for magnetic reconnection events is sometimes determined by defining N as the direction of the gradient across the current sheet and L as the direction of maximum variance of the magnetic field. The third direction, M , is often assumed to be the direction of zero gradient, and thus the orientation of the X line. But when there is a guide field, the X line direction may have a significant component in the L direction defined in this way. For a 2D description, a coordinate system describing such an event would preferably be defined using a different coordinate direction M' oriented along the X line. Here we use a 3D particle-in-cell simulation to show that the X line is oriented approximately along the direction bisecting the asymptotic magnetic field directions on the two sides of the current sheet. We describe two possible ways to determine the orientation of the X line from spacecraft data, one using the minimum gradient direction from Minimum Directional Derivative analysis at distances of the order of the current sheet thickness from the X line, and another using the bisection direction based on the asymptotic magnetic fields outside the current sheet. We discuss conditions for validity of these estimates, and we illustrate these conditions using several Magnetospheric Multiscale (MMS) events. We also show that intersection of a flux rope due to secondary reconnection with the primary X line can destroy invariance along the X line and negate the validity of a two-dimensional description.

Plain Language Summary

At an interface between two regions with magnetic field pointing in different directions, the magnetic fields can reconnect across the interface. While real magnetic reconnection events are three-dimensional, there can sometimes be a direction of approximate invariance, so that a two-dimensional description can be valid. In such cases, it can be beneficial to define a coordinate system with one coordinate along the direction of the smallest gradient in the magnetic field. Using a simulation of magnetic reconnection, we show how the direction of smallest gradient, $\mathbf{e}_{M'}$, is determined, and also discuss how spacecraft observations could be used to find that direction. We also illustrate how the invariant direction can be determined using several events observed by the Magnetospheric Multiscale (MMS) spacecraft.

1 Introduction

While magnetic reconnection events in space are certainly three-dimensional, the plasma sometimes aligns itself in a laminar state that is approximately two-dimensional. If one wanted to conduct a 2D simulation of such an event, it would be important to choose a coordinate system such that the 2D plane of the simulation matched the plane of that event's greatest spatial variation. Furthermore, a two dimensional visualization of the fields can be useful even when the plasma is not approximately two-dimensional. Thus it can be useful to define a coordinate system in which one of the directions is along the direction of the minimum spatial gradient.

Denton et al. (2016, 2018) defined a coordinate system using the maximum gradient direction of Minimum Directional Derivative (MDD) analysis (Shi et al., 2005, 2019) for the normal direction across the current sheet, N , and the maximum variance direction of Maximum Variance Analysis (MVA) (Sonnerup & Cahill, 1967; Sonnerup & Scheible, 1998) for the direction of the reconnecting magnetic field, L , with some adjustment if those directions were not orthogonal (Denton et al., 2018). The M direction was found from the cross product of \mathbf{e}_N and \mathbf{e}_L .

But Denton et al. (2016, 2018) also stated that the direction of minimum gradient from MDD was sometimes more closely aligned with \mathbf{e}_L than with \mathbf{e}_M as defined above. For the purposes of a 2D description, the minimum gradient would ideally be orthog-

onal to the reconnection plane, L - N ; so an L - N plane defined using MVA may not best represent the plane of predominant spatial variation. Recently Pathak et al. (2022) examined this issue for an MMS event and reported that the direction of least gradient was tilted between 40° and 60° from \mathbf{e}_M as defined above, and their work motivated our study. (See also work by Qi et al. (2023).)

Tilting of the X line toward the direction of the maximally varying reconnection magnetic field has been predicted by theory when there is a guide field, that is, a component of the magnetic field in the M direction as defined above (Swisdak & Drake, 2007; Hesse et al., 2013). In a large-scale simulation allowing the X line orientation to develop self consistently (Liu et al., 2018), the X line developed roughly along the angle of bisection between the asymptotic magnetic field directions on the two sides of the current sheet. The orientation based on bisection was similar to that of several other theoretical predictions (Liu et al., 2018), but significantly different from the M direction as defined above. Note also that bisection is used in the Moore et al. model to find the location of the X line along the global magnetopause (Moore et al., 2002; Qudsi et al., 2022).

Here we examine the simulation of Liu et al. (2018) in detail, showing that the MDD minimum gradient direction is in good agreement with the X line orientation within about one half and two ion inertial lengths (or proton inertial lengths, since the only ions in the simulation are protons), d_i , from the X line, where $d_i \equiv c/\omega_{p,i}$, c is the speed of light, $\omega_{p,i} \equiv \sqrt{ne^2/(m_i\epsilon_0)}$ is the ion plasma frequency, n is the ion or electron density (for an H⁺/electron plasma), e is the proton charge, m_i is the proton mass, and ϵ_0 is the permittivity of free space. We also discuss the conditions for which the calculation of the MDD minimum gradient direction can be trusted.

A second approach is to estimate the orientation of the X line using bisection of the asymptotic magnetic field directions on either side of the current sheet. In the simulation studied here, that requires finding the fields at locations at least a few current sheet thicknesses away from the current sheet (Appendix B). But time dependence of the magnetosheath magnetic field will often make this approach infeasible.

We also discuss the problem of determining the orientation of the X line using other methods. Along the way, we demonstrate how to use Maximum Gradient Analysis (MGA) (Shi et al., 2019) to get estimates for the maximum variance (L) direction that in some cases may be better than those found from MVA (Appendix A).

We also show calculations of the MDD minimum gradient direction for several MMS events, including that of Pathak et al. (2022), in order to demonstrate under which conditions that calculation can be trusted to be accurate.

The simulation and MMS data are described in section 2, our analysis methods are described in section 3, simulation results are shown in section 4, and results for MMS events are shown in section 5. Discussion and conclusions follow in section 6.

2 Simulation and data

2.1 Simulation

The particle-in-cell (PIC) simulation of magnetic reconnection at the magnetopause was performed using the electromagnetic simulation code VPIC (Bowers et al., 2009). The mass ratio, m_i/m_e was 25, where m_i and m_e are the ion (proton) and electron mass, respectively. The guide field in the simulation was normalized to be unity in the y direction. The reconnecting component in the x direction was -0.5 at low z values (hereafter referred to as the magnetosheath), and 1.5 at high z values (hereafter referred to as the magnetosphere). The half thickness of the hyperbolic tangent current sheet was $0.8 d_i$.

118 The simulation was three-dimensional with a very large box size, $(L_x, L_y, L_z) = (256,$
 119 $256, 24) d_i$, where L_i is the length in the i th direction, but we will use a smaller section
 120 of data with dimensions $(L'_x, L'_y, L'_z) = (30, 90, 16) d_i$. The original grid point separation
 121 was $0.0625 d_i = 0.313 d_e$, though the data that we used was down sampled by a
 122 factor of 2 in each direction. The boundary conditions were periodic in the x and y
 123 directions, and in the z direction, the boundary condition was perfectly conducting for the
 124 fields and reflecting for particles.

125 The simulation was initialized with a small and localized (within about two d_i in
 126 the y direction) perturbation favoring reconnection with an X line along the y direction,
 127 but the reconnection subsequently developed so that the X line developed along another
 128 direction. This direction is in the x - y plane, but is rotated counterclockwise from the y
 129 direction by the angle θ_{Xline} .

130 2.2 MMS data

131 In addition to analyzing simulation data, we will use magnetic field measurements
 132 from the MMS mission (Burch et al., 2015). The fluxgate magnetometer (FGM) (Russell
 133 et al., 2016) and search coil magnetometer (SCM) (Le Contel et al., 2016) data are com-
 134 bined into a single product with original resolution of 0.12 ms (Fischer et al., 2016; Ar-
 135 gall et al., 2018). We boxcar average this to much lower resolution, typically 0.05 s. (Us-
 136 ing the high resolution data eliminates inaccuracies related to shifting spacecraft mag-
 137 netic field data to common times.) For purposes of a reconstruction of the magnetic field
 138 (Denton et al., 2020, 2022), we sometimes use the particle current density, \mathbf{J} , from the
 139 burst mode ion and electron bulk velocity moments from the Fast Plasma Instrument
 140 (FPI) (Pollock et al., 2016).

141 3 Methods

142 3.1 MDD and MGA

143 We will find that the direction of the simulation X line is well described by the min-
 144 imum gradient direction from MDD (Shi et al., 2005, 2019), if it can be calculated ac-
 145 curately at locations close to the X line. To implement MDD, one first constructs a ma-
 146 trix from the gradient of the vector magnetic field, \mathbf{M}_{gb} , where g represents a compo-
 147 nent of the spatial derivative, and b represents a component of the magnetic field. Then
 148 one multiplies by the transpose of \mathbf{M}_{gb} , \mathbf{M}_{gb}^T , to get $\mathbf{M}_{\text{MDD}} = \mathbf{M}_{gb} \mathbf{M}_{gb}^T$, and solves the
 149 eigenvalue problem. This procedure yields three eigenvectors, which are the directions
 150 of the maximum, intermediate, and minimum gradient of the magnetic field. In the orig-
 151 inal formulation, which we use, the eigenvalues are the squared values of the gradient
 152 in those directions. We expect the maximum gradient direction for our simulation to be
 153 z , since the equilibrium field only varies with respect to z .

154 Maximum Gradient Analysis (MGA) (Shi et al., 2019), is similar, but the matrix
 155 analyzed is $\mathbf{M}_{\text{MGA}} = \mathbf{M}_{gb}^T \mathbf{M}_{gb}$. The eigenvalues are the same as those for MDD, but
 156 this analysis finds the eigenvectors of maximum, intermediate, and minimum variance
 157 of the magnetic field. Our tests have shown that MGA yields a similar result to that of
 158 Maximum Variance Analysis (MVA) (Sonnerup & Cahill, 1967; Sonnerup & Scheible,
 159 1998), where instead of a time series of magnetic field vectors, one uses the magnetic field
 160 vectors measured by the four MMS spacecraft at one time. Since only the x component
 161 of the equilibrium field varies, we expect the maximum variance direction to be x . We
 162 will also use standard MVA analysis, and the expected result is the same, maximum vari-
 163 ance in the x direction.

164 For the simulation, an (L, M, N) coordinate system found using MDD for \mathbf{e}_N , MVA
 165 or MGA for \mathbf{e}_L , and $\mathbf{e}_M = \mathbf{e}_N \times \mathbf{e}_L$ would be similar to the original simulation coor-

166 dinate system, (x,y,z) , for which B_y is uniform, and we will consider these to be equiv-
 167 alent.

168 For the most part, when we write MDD or MGA, we mean MDD or MGA using
 169 the magnetic field (MDDB or MGAB), but we sometimes use these acronyms to refer
 170 to the techniques, which may be applied to other fields as well.

171 3.2 Calculation of the MDD minimum gradient direction for MMS events

172
 173 For MMS events, calibration errors in the magnetic field, that is, constant offsets
 174 measured by one spacecraft relative to another spacecraft, lead to constant errors in the
 175 gradient of the magnetic field which could invalidate the MDD directions (Denton et al.,
 176 2010). But in order to determine the minimum gradient direction accurately, it is not
 177 necessary to measure the magnitude of the minimum gradient accurately. What is es-
 178 sential is that the orientation of the plane containing the maximum and intermediate gra-
 179 dient directions, \mathbf{e}_N and $\mathbf{e}_{L'}$ respectively, be accurately determined. In that case, with
 180 MDD yielding the three orthogonal directions, \mathbf{e}_N , $\mathbf{e}_{L'}$, and $\mathbf{e}_{M'}$, the minimum gradi-
 181 ent direction $\mathbf{e}_{M'}$ will automatically be perpendicular to the L' - N plane.

182 The magnetic field measured by the MMS spacecraft is calibrated to be accurate
 183 to 0.1 nT (Russell et al., 2016). Assuming a spacecraft spacing d_{sc} , contamination of the
 184 gradient could occur for gradient values on the order of $0.1 \text{ nT}/d_{sc}$. Considering that the
 185 MDD eigenvalues are the squared gradient, that means that the MDD eigenvalues must
 186 be significantly greater than $(0.1 \text{ nT}/d_{sc})^2$ for a particular direction in order to deter-
 187 mine that eigenvector accurately (Denton et al., 2020).

188 In order to determine the minimum gradient direction accurately, we need the MDD
 189 maximum and intermediate gradient eigenvalues to be significantly greater than this amount,
 190 ideally at least roughly a factor of 10. And we also need a large ratio of the intermedi-
 191 ate gradient eigenvalue to the minimum gradient eigenvalue, at least roughly a factor of
 192 10, so that these directions are well differentiated. Otherwise the two directions do not
 193 correspond to significantly different gradients. It would be better for these factors to be
 194 even higher. The eigenvalues are proportional to the squared gradient, so a factor of 10
 195 corresponds to a factor of only 3.2 in the gradient.

196 Assuming these conditions are met, the minimum gradient direction can be deter-
 197 mined from MDD. Note that it is not necessary for the MDD maximum gradient direc-
 198 tion to be well differentiated from the MDD intermediate gradient direction, only that
 199 both of these gradients are well above the gradient of possible calibration errors, and that
 200 both of these directions are well differentiated from the MDD minimum gradient direc-
 201 tion. In this case, the sum of the gradients in the maximum and intermediate gradient
 202 directions will be calculated accurately, defining the plane orthogonal to the minimum
 203 gradient direction, and that plane will be well differentiated from the minimum gradi-
 204 ent direction. In other words, the maximum and intermediate gradient eigenvalues should
 205 both be roughly greater than at least 10 times $(0.1 \text{ nT}/d_{sc})^2$, and the minimum gradi-
 206 ent eigenvalue should be roughly at least a factor of 10 below the intermediate gradient
 207 eigenvalue.

208 A final indication of consistency would be that the time-dependent minimum gra-
 209 dient direction, \mathbf{e}_m , is roughly constant. Of course there may be some time dependence,
 210 but if that direction varies wildly, it suggests that it may not be well determined.

211 3.3 Polynomial reconstruction

212 Using the four MMS spacecraft measurements of magnetic field, we can do a lin-
 213 ear reconstruction of the magnetic field using the “3-D linear with only \mathbf{B} as input”, or

214 “LB-3D”, model of Denton et al. (2020). This 12 parameter model is almost equivalent
 215 to the results of MDD. The slight difference is because LB-3D enforces $\nabla \cdot \mathbf{B} = 0$. Be-
 216 cause the reconstruction gradient of the magnetic field is almost the same as the actual
 217 gradient, the model magnetic field at the spacecraft locations is almost exactly the same
 218 as the observed fields. This method is the same or nearly the same as the First Order
 219 Taylor Expansion (FOTE) method of Fu et al. (2015, 2016, 2020). Here we use the method
 220 of Denton et al. (2022) that uses input data from multiple times to get improved recon-
 221 structions.

222 4 Simulation results

223 4.1 X Line Orientation and the Minimum Gradient Direction

224 Figure 1 shows two-dimensional cuts of several quantities through the simulation.
 225 In figures such as Figure 1 that have labels that are a combination of an uppercase let-
 226 ter followed by a lowercase letter, like “(Aa),” we will use the following convention. Fig-
 227 ures 1A represents the set of panels in the first row of panels, Figures 1a represents the
 228 set of panels in the first column of panels, and Figure 1Aa represents the single panel
 229 in the first row and first column (upper left panel). Figures 1a show two dimensional cuts
 230 of the magnitude of the current density, J .

231 Figure 1Aa shows a two-dimensional cut of J in the x - y plane at $z = 3.75 d_i$ (a
 232 subset of the x - y plane of Figures 2b–2e of Liu et al. (2018) with the same coordinate
 233 values). The diagonal dashed green line in Figure 1Aa roughly goes along the peak of
 234 the current density, as indicated by the dark color. This line is at an angle $\theta_{\text{Xline}} = -14.6^\circ$
 235 from y measured counterclockwise toward negative x (or 14.6° measured clockwise to-
 236 ward positive x). This angle is very close to -14.9° , which results from the bisection (av-
 237 erage direction found from the average of the unit vectors) of the magnetosheath and
 238 magnetosphere fields, $(B_x, B_y, B_z) = (-0.5, 1, 0)$ and $(1.5, 1, 0)$, respectively. We will call
 239 this peak in the current density the X line. It is the primary X line, by which we mean
 240 an X line that extends over the largest scale and has inflow from the two sides of the cur-
 241 rent sheet. (But note that secondary reconnection may occur within the exhaust of the
 242 primary X line.) Based on the peak in current density, it is the position of the maximum
 243 gradient in the magnetic field, but not necessarily the exact position of a reversal in the
 244 components of the magnetic field in the plane perpendicular to the X line.

245 Figure 1Ba shows a two dimensional cut of J in the z - y plane along the diagonal
 246 dashed green line in Figure 1Aa. The peak value of J is at $z = 3.75 d_i$, indicated by
 247 the vertical dashed green line in Figure 1Ba.

248 Figure 1Ca shows a two dimensional cut of J in the x - z plane (the usual “recon-
 249 nection plane”) at $y = 60 d_i$, while Figure 1Da shows the same view at $y = 30 d_i$. These
 250 y locations are indicated by the horizontal green lines in Figures 1Aa and Figures 1Ba.

251 Figures 1b (second column of panels) shows the same two dimensional cuts as Fig-
 252 ures 1a, but now showing the normal component of \mathbf{B} , B_z . As indicated by the color scales,
 253 red values are positive, blue values are negative, and white indicates zero value. B_z re-
 254 verses as the X line is crossed in the x direction (Figures 1Ab, 1Cb, and 1Db). B_z is small
 255 at different values of z above and below the X line (Figure 1Bb), except for values of y
 256 between about $60 d_i$ and $80 d_i$, where the current also seems to be distorted (Figure 1Aa);
 257 we will discuss this region later.

258 We now calculate the MDD minimum gradient eigenvector on the simulation grid.
 259 While we could introduce virtual spacecraft to calculate the derivatives using a tetra-
 260 hedron, here we simply use centered second order accurate finite differences on the grid.
 261 Based on the grid separation of the data that we used, $0.125 d_i$, the effective spacecraft
 262 separation would be about $0.2 d_i$. In Figures 1c we show $\theta_{\text{MDDmin},z}$, which is the angle

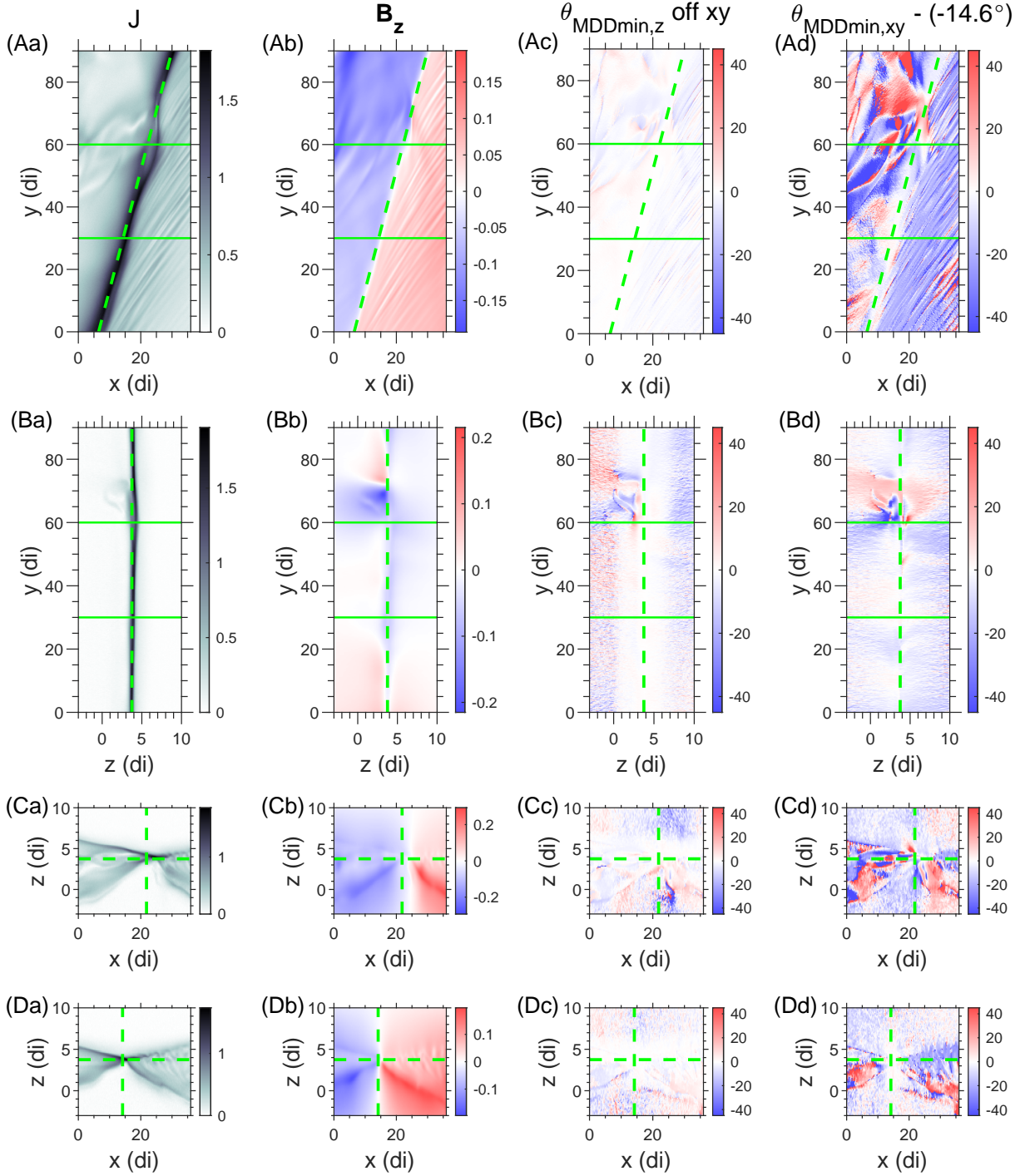


Figure 1. 2D simulation cuts showing the orientation of the X line and the relation to the MDD minimum gradient direction. In rows (A–D) are (A) 2D cuts in the x - y plane at $z = 3.75 d_i$, (B) 2D cuts in the z - y planes at varying y values along the diagonal dashed green line in panel (Aa), and (C–D) 2D cuts in the x - z plane at (C) $y = 60 d_i$ and (D) $y = 30 d_i$. In columns (a–d) are plotted (a) the magnitude of the current density, J , (b) B_z , (c) the angle of the minimum gradient direction off of the x - y plane (positive toward positive z), $\theta_{\text{MDDmin},z}$, and (d) the angle of the minimum gradient direction in the x - y plane counterclockwise from the y direction minus the angle to the X line, $\theta_{\text{MDDmin},xy} - (-14.6^\circ)$. The dashed green lines are either along or through the X line, while the upper and lower horizontal solid green lines are the locations of cuts across the X line at $y = 60 d_i$ and $30 d_i$, respectively.

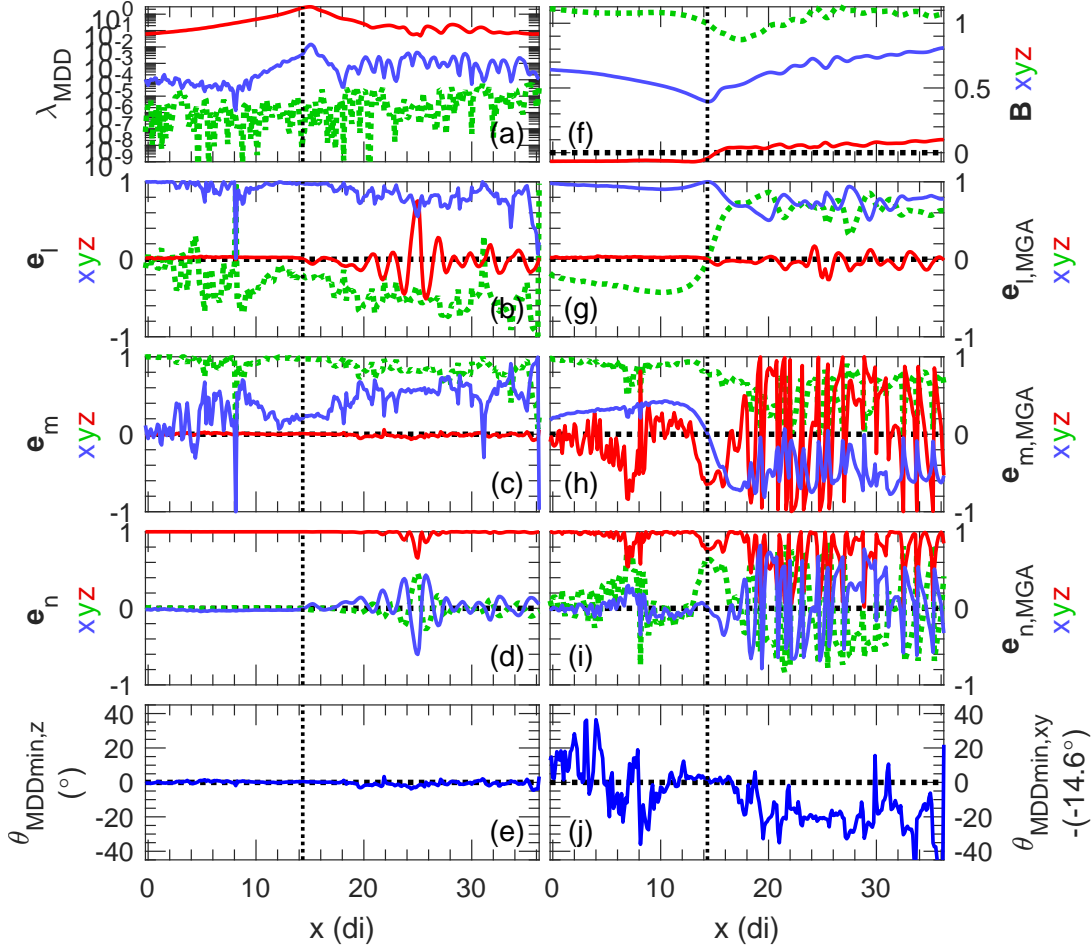


Figure 2. Variation of MDD and MGA quantities for x varying across the X line at $(y,z) = (30,3.75) d_i$. (a) MDD eigenvalues; (b–d) MDD eigenvectors in the (b) intermediate gradient, (c) minimum gradient, and (d) maximum gradient directions; (e) $\theta_{\text{MDDmin},z}$; (f) \mathbf{B} ; (g–i) MGA eigenvectors in the (g) maximum variance, (h) intermediate variance, and (i) minimum variance directions; and (j) $\theta_{\text{MDDmin},xy} - (-14.6^\circ)$. The vertical dotted black line is at the X line at $z = 3.75 d_i$.

263 that the minimum gradient direction makes away from the x - y plane, positive toward
 264 positive z . This angle is generally small within several d_i of $z = 3.75 d_i$, except for val-
 265 ues of z less than $3.75 d_i$ for y between about $60 d_i$ and $77 d_i$ (Figures 1Bc and 1Cc)

266 We now show the angle of the minimum gradient direction within the x - y plane.
 267 We define $\theta_{\text{MDDmin},xy}$, like θ_{Xline} mentioned previously, as the angle counterclockwise from
 268 the y direction. In Figures 1d, we show $\theta_{\text{MDDmin},xy} - \theta_{\text{Xline}} = \theta_{\text{MDDmin},xy} - (-14.6^\circ)$.
 269 Except for the region between about $y = 60$ and $77 d_i$ (which includes the plane shown
 270 in Figure 1Cd), the difference of the two angles is small within x values of about 2 or
 271 3 d_i from the X line, and at larger separations in z from the X line.

272 We examine this further in Figures 2 and 3. Figure 2 shows 1D plots of various quan-
 273 tities for x varying across the X line at $(y,z) = (30,3.75) d_i$ (along the lower horizontal
 274 green line in Figure 1Aa). Figure 3 shows the same quantities for z varying across the
 275 X line at $(x,y) = (14.33,30) d_i$ (along the lower horizontal solid green line in Figure 1Ba).

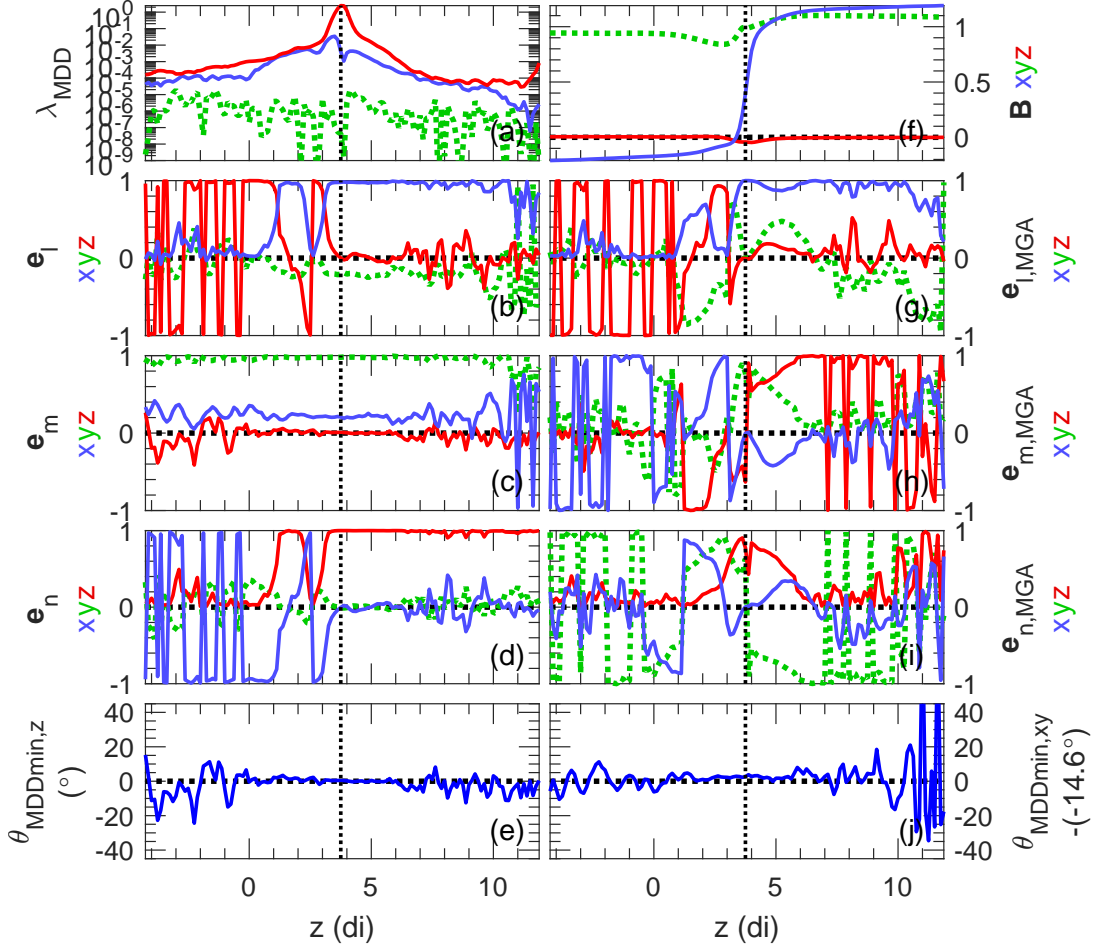


Figure 3. Variation of MDD and MGA quantities for z varying across the X line at $(x,y) = (14.33,30) d_i$. Otherwise, the format is similar to that of Figure 2.

Figure 2a shows the MDD eigenvalues, or the squared gradient of the vector magnetic field in the maximum gradient (red curve), intermediate gradient (blue curve), and minimum gradient (dotted green curve) directions. Figures 2b–2d show (b) the MDD intermediate gradient eigenvector, \mathbf{e}_l , (c) the MDD minimum gradient eigenvector, \mathbf{e}_m , and (d) the MDD maximum gradient eigenvector, \mathbf{e}_n in terms of x (blue curve), y (dotted green curve), and z (red curve) components. If the maximum gradient direction were the direction across the current sheet, N , and the minimum gradient direction were the direction orthogonal to N and the direction of maximum magnetic field variance, L , then l , m , and n would be expected to be close to L , M , and N , or x , y , and z .

There is always a good separation between the maximum and intermediate gradient eigenvalues (red and blue curves in Figure 2a), and the maximum gradient direction (Figure 2d) is usually close to the z direction, which is the direction of the gradient in the equilibrium magnetic field. There is significant variation in the minimum gradient direction (Figure 2c), but near the crossing of the X line at the vertical black dotted line, the minimum gradient direction is predominantly in the y direction (dotted green curve), but with a positive x component (blue curve). This is what we would expect based on the tilt of the dashed green line (Figure 1Aa) toward positive x .

Figure 2e shows $\theta_{\text{MDDmin},z}$, and indicates that the minimum gradient direction is in the x - y plane all across the current sheet at this y value. Figure 2j shows $\theta_{\text{MDDmin},xy} - (-14.6^\circ)$. This value indicates that the orientation of the minimum gradient direction within the x - y plane varies, but that $\theta_{\text{MDDmin},xy}$ (the angle of the minimum gradient counterclockwise from y) is very close to $\theta_{\text{Xline}} = -14.6^\circ$ (the angle of the X line counterclockwise from y) within $2 d_i$ of the X line (vertical black dotted line).

Figure 2f shows the magnetic field components along x and Figures 2g–2i show the MGA maximum variance direction, $\mathbf{e}_{l,\text{MGA}}$, the MGA intermediate variance direction, $\mathbf{e}_{m,\text{MGA}}$, and the MGA minimum variance direction, $\mathbf{e}_{n,\text{MGA}}$, respectively. Since MGA provides a local approximation to MVA, l_{MGA} , m_{MGA} , and n_{MGA} would be expected to be similar to x , y , and z . There is considerable variation in these directions, but $\mathbf{e}_{l,\text{MGA}}$ is in the x direction (as indicated by the blue curve in Figure 2g) at the crossing of the X line (vertical dotted black line).

Figure 3 plots the same quantities as in Figure 2, but for z varying across the X line at $(x,y) = (14.33,30) d_i$ (along the lower horizontal solid green line in Figure 1Ba). Figure 3f shows the reversal of B_x across our X line (position of maximum current density) indicated again by the vertical black dotted line.

The MDD maximum gradient direction (Figure 3d) is consistently in the z direction for $z > 3.3 d_i$, but varies for smaller values of z . Perhaps surprisingly, the most consistent direction is that of the MDD minimum gradient (Figure 3c). This is because the separation between the intermediate and minimum gradient eigenvalues in Figure 3a is greater than that between the maximum and intermediate gradient eigenvalues. Both $\theta_{\text{MDDmin},z}$ and $\theta_{\text{MDDmin},xy} - (-14.6^\circ)$ are close to zero within at least $3 d_i$ of the X line crossing.

The MGA eigenvector directions (Figures 3g–3i) are more variable, but similar to Figure 2g, Figure 3g shows that the maximum variance direction is in the x direction (blue curve) at the X line crossing.

Thus for this simulation the minimum gradient direction gives us the direction along the X line at locations near the X line (within about $2 d_i$ in x , and within about $3 d_i$ in z), except in the region between about $y = 60 d_i$ and $80 d_i$, as seen in Figures 1c and 1d. We will discuss this region further below.

Note that the distances $2 d_i$ and $3 d_i$ are of the order of the thickness of the equilibrium current layer, $1.6 d_i$ (section 2.1).

326 We tried using MDD with other vector quantities from the simulation. MDD us-
 327 ing the electron velocity, \mathbf{V}_e (MDDVe), or the current density, \mathbf{J} (MDDJ), yielded simi-
 328 lar results to MDD using the magnetic field (MDD).

329 On the other hand, MDD using the simulation ion velocity (MDDVi) or electric
 330 field (MDDE) was not useful. We got much better results for these if we averaged the
 331 simulation data over all three directions using 343 data points, showing that there was
 332 some information about the gradient in the fields; but it would be impossible to do that
 333 kind of averaging for spacecraft data (at least with current missions). Smoothing the data
 334 in only one direction by averaging over 31 data points (a distance of $3.75 d_i$, which is more
 335 than two current sheet thicknesses ($1.6 d_i$)) did not lead to a consistently accurate di-
 336 rection for the X line; and this was true whether the averaging was done in the x , y , or
 337 z directions. Results are shown in the Supplementary Information (Text S1 and Figures S1-
 338 S13).

339 4.2 Other calculations

340 Appendix A shows how MDD and MGA are used over intervals of simulation data
 341 to determine the maximum gradient and maximum variance directions. The MDD max-
 342 imum gradient direction is very well determined. The maximum variance direction is not
 343 as well determined. We find that MGA under some circumstances gives a better mea-
 344 sure of the maximum variance direction than does MVA, particularly when the trajec-
 345 tory of the spacecraft does not cross the current sheet. But none of these calculations
 346 gives us the orientation of the X line.

347 We also consider in Appendix A other quantities like the current density or elec-
 348 tron velocity. Genestreti et al. (2018) used the direction of maximum variance of the elec-
 349 tron velocity to get the \mathbf{e}_L , but we find here that that approach does not yield the L di-
 350 rection for the simulation data.

351 Based on the theoretical results of Liu et al. (2018), it is not surprising that bisection
 352 can be used with simulation data to get the M' direction. Considering the initial-
 353 ization of the simulation, all we would have to do is to use the asymptotic magnetic field
 354 far enough from the current sheet so as not to be affected by the reconnection. But in
 355 order to demonstrate how the bisection direction might be calculated, we use cuts of sim-
 356 ulation data to estimate the M' direction in the Supplementary Information (Text S2
 357 and Figure S14).

358 5 Results for MMS Events

359 Here we examine the use of MDD to find the minimum gradient direction for sev-
 360 eral MMS events, including that studied by Pathak et al. (2022).

361 5.1 MDD minimum gradient direction for several well-known MMS events

362
 363 Figure 4 presents the MDD eigenvectors and MGA maximum variance direction
 364 for three well-known MMS events, the Torbert et al. (2018) magnetotail reconnection
 365 event (Figures 4a), and the Burch et al. (2016) (Figures 4b) and Chen et al. (2017) (Fig-
 366 ures 4c) magnetopause reconnection events. The L - M - N coordinate systems used here
 367 are described in Appendix B. Our main purpose in this subsection is to illustrate the
 368 conditions under which the MDD minimum gradient direction can be reliably determined.

369 Consider first the event of Torbert et al. (2018) presented in Figures 4a. The co-
 370 ordinate system used for this event was based on MDD (Appendix B), so it's not sur-
 371 prising that the MDD local (time-dependent) intermediate, minimum, and maximum gra-

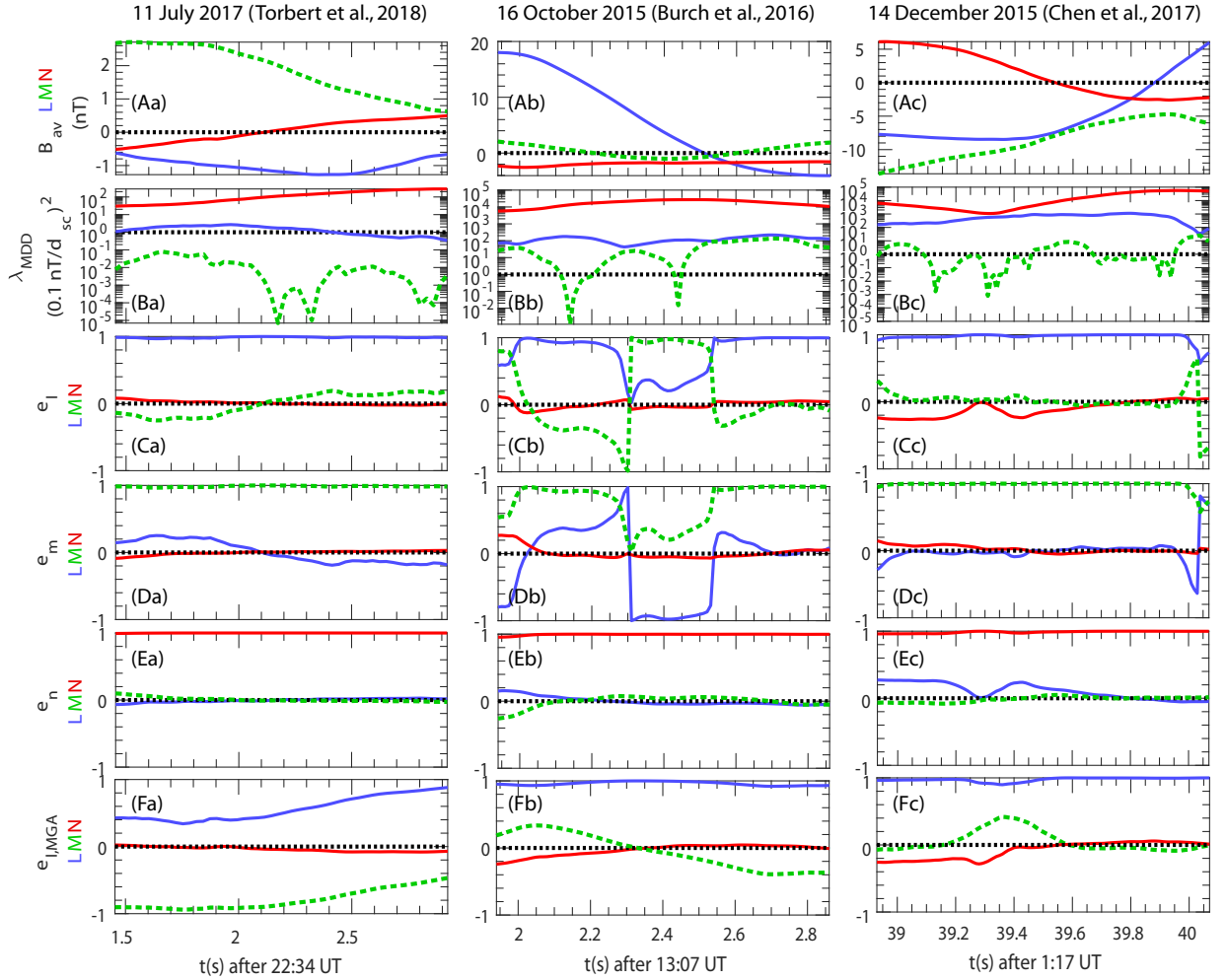


Figure 4. MDD and MGA directions for three well-known MMS events. For (a) the Torbert et al. (2018) magnetotail reconnection event, and the (b) Burch et al. (2016) and (c) Chen et al. (2017) magnetopause reconnection events, (A) the magnetic field averaged over the four MMS spacecraft, (B) the MDD maximum, intermediate, and minimum eigenvalues, (C–E) the MDD time-dependent eigenvectors for the (C) intermediate, (D) minimum, and (E) maximum gradient directions, and (F) the MGA time-dependent maximum variance eigenvalue.

372 dent directions, \mathbf{e}_l , \mathbf{e}_m , and \mathbf{e}_n , are mostly in the L , M , and N directions, respectively.
 373 However, although the minimum gradient direction is well differentiated from the inter-
 374 mediate gradient direction, based on the ratio between the intermediate gradient eigen-
 375 value (blue curve in Figure 4Ba) and the minimum gradient eigenvalue (dotted green curve
 376 in Figure 4Ba), the intermediate gradient eigenvalue is close to the possible value from
 377 calibration errors (dotted horizontal line in Figure 4Ba). So it is not large enough in order
 378 to trust that the intermediate gradient is measured accurately, as discussed in section
 379 3.2. Consequently we can't be sure that the maximum and intermediate directions
 380 define the plane of the largest gradients.

381 Next consider the event of Burch et al. (2016) in Figures 4b. The coordinate system
 382 was based on the hybrid method using MVA for L and MDD for N . Consequently
 383 $\mathbf{e}_{l,MGA}$ (the local MGA maximum variance direction) is mostly in the L direction (Fig-
 384 ure 4Fb) and \mathbf{e}_n is mostly in the N direction (Figure 4Eb). In this case, both the max-
 385 imum and intermediate gradients are large (based on the red and blue curves in Figure 4Bb).
 386 But for most of the time, the minimum gradient direction is not well differentiated from
 387 the intermediate gradient direction, seeing as the dotted green curve in Figure 4Bb is
 388 close to the blue curve. A possible exception is at a small segment of time around $t =$
 389 2.15 s, but because of the time averaging of the original data (over 0.5 s), this segment
 390 of time is not big enough to get a reliable direction.

391 Finally consider the event of Chen et al. (2017) shown in Figures 4c. Here the co-
 392 ordinate system was based on MDD, so as in Figures 4a, \mathbf{e}_l , \mathbf{e}_m , and \mathbf{e}_n , are mostly in
 393 the L , M , and N directions, respectively. In this case, both conditions are met. Both
 394 the maximum and intermediate gradients are calculated accurately (based on the large
 395 maximum and intermediate eigenvalues in Figure 4Bc), and the minimum gradient eigen-
 396 value is well separated from the intermediate gradient eigenvalue (based on the separa-
 397 tion of the blue curve and dotted green curve in Figure 4Bc). Therefore in this case, the
 398 minimum gradient direction can be calculated accurately, and that direction is roughly
 399 constant as indicated by the time-dependent \mathbf{e}_m (Figure 4Dc), except at the very end
 400 of the time interval shown (where the minimum gradient eigenvalue in Figure 4Bc is close
 401 to the intermediate gradient eigenvalue).

402 In Figure 5, we show a reconstruction of the magnetic field in the L - N and L - M
 403 planes at eight different times using the linear “LB-3D” model of Denton et al. (2020).
 404 (For this plot, we used boxcar smoothing of the magnetic field over 0.5 s, and multiple
 405 input times over a range of 0.14 s (Denton et al., 2022).) Because the model is linear,
 406 the results are almost equivalent to those from MDD, but the reconstruction is useful
 407 for visualizing the magnetic structure. In Figures 5B–5E, the lower case letters “a” though
 408 “h” in the panel labels refer to those times labeled with the same letters in Figure 5A.
 409 In Figures 5B and 5D, plots are shown in the L - N plane at $M = 0$, where the origin
 410 is at the centroid of the MMS spacecraft. The gold X symbols mark a magnetic mini-
 411 mum of the magnitude of the magnetic vector in the L - N plane, which is at the X line.
 412 In Figures 5C and 5E, plots are shown in the L - M plane at the N values of the mag-
 413 netic minima shown in Figures 5B and 5D.

414 Because B_L is small at the magnetic minima in Figures 5B and 5D, the magnetic
 415 field lines (black curves) in the L - M plane (Figures 5C and 5E) are vertical at the X sym-
 416 bols. (The reason that the field lines curve at L and M values away from the X line, is
 417 because the current sheet is somewhat tilted; that is, the current sheet is not exactly at
 418 constant N .) Also, the color is white at those symbols, because B_N is zero. The centroid
 419 of the MMS spacecraft passes closest to the X line in the L direction at $t = 39.45$ s (Fig-
 420 ure 5Bb). And at that time the X line (white color in Figures 5C and 5E) is roughly ver-
 421 tical; that is, it is roughly aligned with \mathbf{e}_M . This is approximately the case also at the
 422 other times.

Therefore the reconstruction shows a result consistent with Figures 4Dc, that the X line is approximately oriented parallel to \mathbf{e}_M . We chose to use a linear reconstruction because the model magnetic field almost exactly matches the observed field, and because the solutions are better behaved, avoiding strange behavior far from the spacecraft locations. (Polynomial reconstruction does not always give accurate results (Denton et al., 2022).) But if we use the “3D Reduced Quadratic” model of Denton et al. (2020), which uses the current density from the MMS FPI instrument, the reconstruction also shows that the X line is approximately parallel to \mathbf{e}_M when the spacecraft are closest to the X line (not shown).

5.2 MDD minimum gradient direction for the Pathak et al. event

Now we do our own analysis for the event studied by Pathak et al. (2022). Our results for the minimum gradient direction are shown in Figure 6. While we agree with Pathak et al. (2022) that the orientation of the X line can be different than the direction \mathbf{e}_M given by the cross product of the maximum gradient and maximum variance directions, N and L respectively, our results for the difference between these two directions are very different.

To define an L - M - N coordinate system, we used MGA for the L direction, and MDD for the N direction, as described in Appendix C. We smoothed the data with a boxcar average over 0.8 s, but the results are not very different with less smoothing. The maximum to intermediate eigenvalue for both of these directions was 123, and they were within 0.4° of being orthogonal, so only a small adjustment of these directions was needed (Denton et al., 2018). Figure 6d shows that the MDD local time-dependent direction \mathbf{e}_n is very consistent, and mostly in the N direction. Figure 6g shows that the MGA local time-dependent direction $\mathbf{e}_{l,MGA}$ is more variable, but on average is in the L direction, and especially in the middle of the time period between $t = 24.5$ s and $t = 26$ s. Note that the centroid of the MMS spacecraft appears to pass by the X line in the L direction (as suggested by the reversal in $B_{N,av}$ in Figure 6f) at about $t = 26$ s.

A linear (LB-3D) reconstruction of the magnetic field, shown in Figure 7 also indicates that the spacecraft passed nearest to the X line at about $t = 26$ s (Figures 7Bd and 7De). (For this plot, we used boxcar smoothing of the magnetic field over 1 s, and multiple input times over a range of 0.1 s.)

Now, returning to Figure 6, the local time-dependent MDD minimum gradient direction, \mathbf{e}_m , is shown in Figure 6c. First note that there are few, if any, times for which the conditions discussed in section 3.2 for accurate determination of the minimum gradient direction are satisfied. The intermediate gradient eigenvalue (blue curve in Figure 6a) is only greater than 10 times $(0.1 \text{ nT}/d_{sc})^2$ from about $t = 23.2$ s to 23.8 s and perhaps momentarily at about $t = 27$ s. And the times for which the minimum gradient eigenvalue (green curve in Figure 6a) is much smaller than the intermediate gradient eigenvalue are limited. Nevertheless, we will discuss the direction of the minimum gradient eigenvector as determined by MDD.

From about $t = 23.2$ s to 23.5 s, both conditions for accurate determination of the minimum gradient direction (large intermediate gradient eigenvalue and large ratio between the intermediate and minimum gradient eigenvalues) are minimally met. At that time, the minimum gradient eigenvector (Figure 6c) is closest to the L direction (based on maximum variance of the magnetic field), as was found in some previous studies (Denton et al., 2016, 2018). But as suggested by Figure 7, MMS was not close to the X line at that time, at least on the scale of the spacecraft separation, and results in section 4.1 suggest that the MDD minimum gradient eigenvector is only along the X line at locations close to the X line.

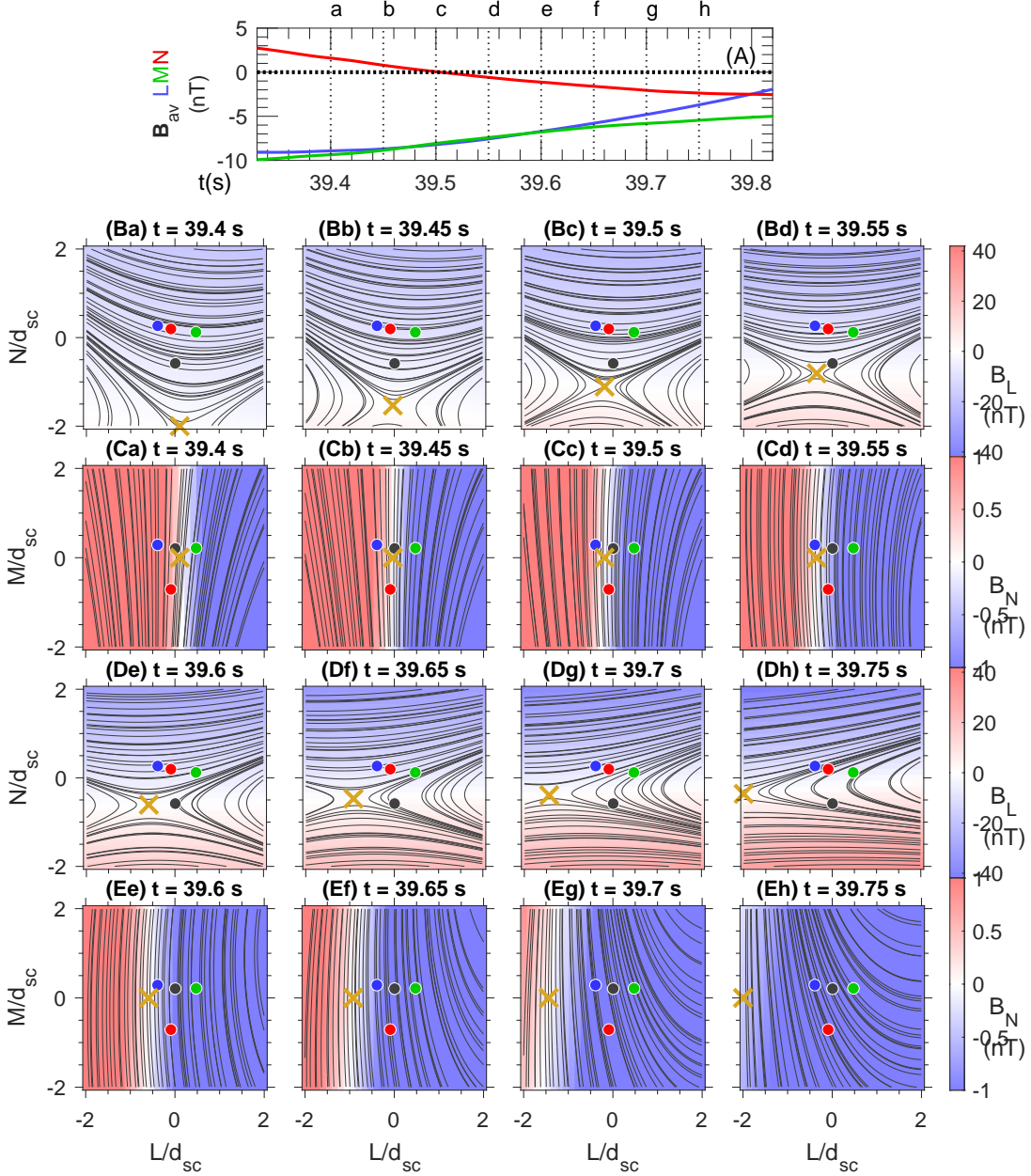


Figure 5. Linear reconstruction of the magnetic field in the $L-N$ and $L-M$ planes for the event of Chen et al. (2017) on 14 Dec 2017 at 01:17 UT. (A) Magnetic field averaged over the four MMS spacecraft, B_{av} , showing the times of the two-dimensional representations of the magnetic field in rows B–E. Reconstructed magnetic streamlines (black) in (B and D) the $L-N$ plane at $M = 0$ (M value of spacecraft centroid) and (C and E) the $L-M$ plane at the N value of the X line in the $M = 0$ plane (gold X symbol in rows B and D). The color scale shows (B and D) B_L and (C and E) B_N . The positions of the MMS spacecraft relative to the spacecraft centroid (origin of each panel) are indicated by the black, red, green, and blue circles for spacecraft 1, 2, 3, and 4.

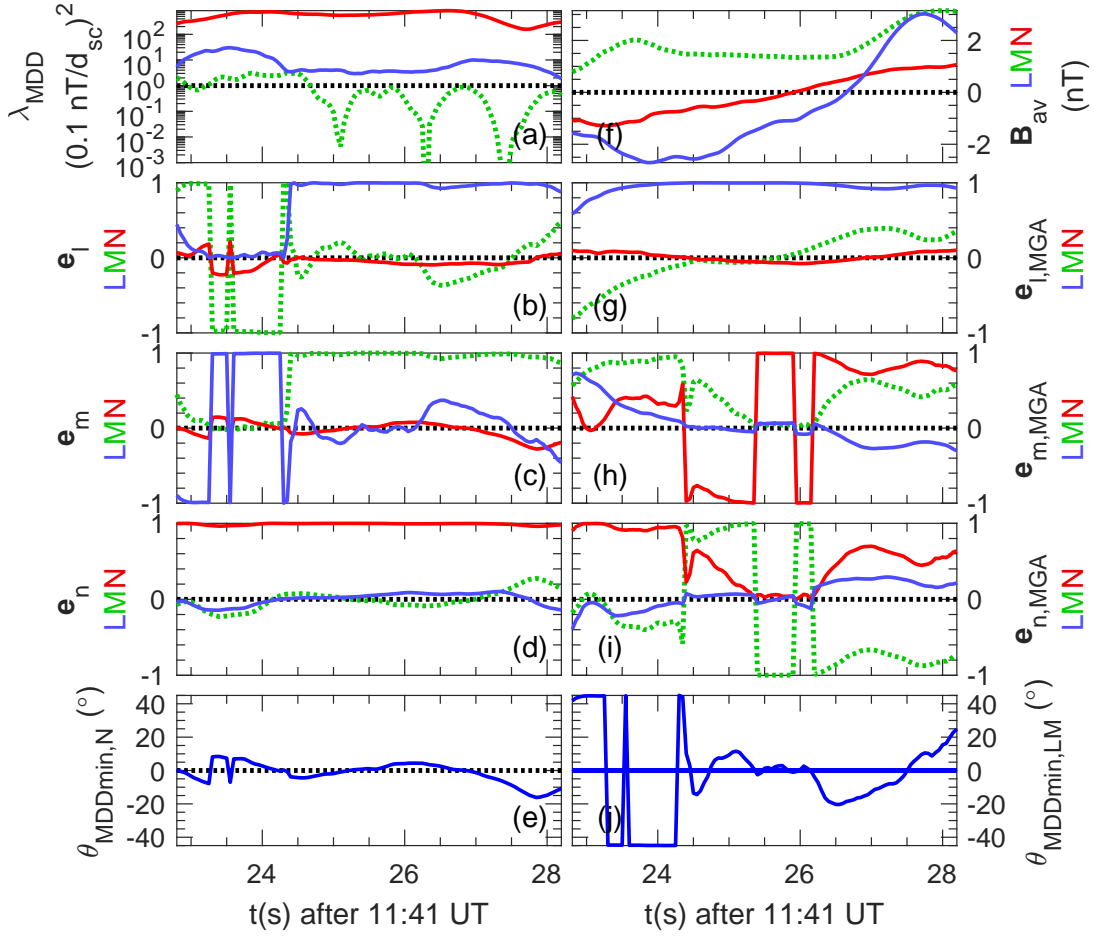


Figure 6. MDD and MGA directions for the event of Pathak et al. (2022) on 27 Aug 2018. The format is similar to that of Figure 2, except that results are shown versus time in s after 11:41 UT, the magnetic field, \mathbf{B}_{av} in panel (f), is averaged over the four MMS spacecraft, the angle $\theta_{MDDmin,LM}$ is measured counterclockwise from the M direction toward the $-L$ direction, and $\theta_{MDDmin,LM}$ itself is shown without subtracting the (unknown) angle to the X line.

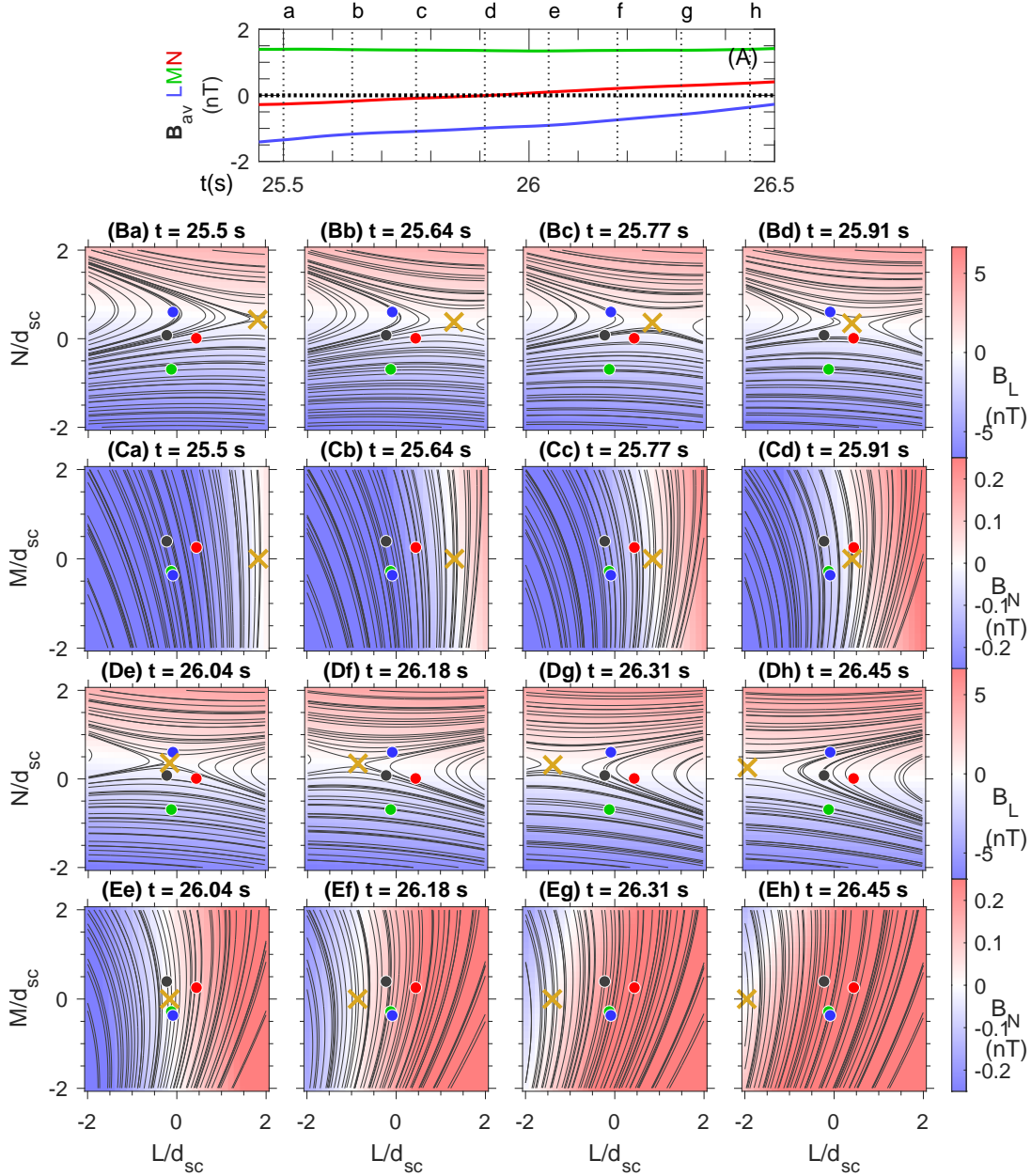


Figure 7. Linear reconstruction of the magnetic field for the event of Pathak et al. (2022) on 27 Aug 2018 at 11:41 UT. The format is the same as that of Figure 5

472 When the MMS spacecraft passed closest to the X line at about $t = 26$ s, as sug-
 473 gested by B_N in Figure 6f and Figures 7Bd and 7De, the conditions of section 4.1 are
 474 not well met. The intermediate gradient eigenvalue and the ratio between the interme-
 475 diate and minimum gradient eigenvalues are not big enough (Figure 6a). Nevertheless,
 476 we note that at that time the time-dependent MDD minimum gradient eigenvector, \mathbf{e}_m ,
 477 is not far off from the M direction (Figure 6c). Figure 6e shows that at that time \mathbf{e}_m
 478 is tilted several degrees toward positive N , and Figure 6j shows that the projection of
 479 \mathbf{e}_m onto the L - M plane is close to the M direction. We find that at that time the MDD
 480 minimum gradient direction is no more than about 5° off from the M direction, very dif-
 481 ferent from the 40° to 60° difference reported by Pathak et al. (2022). Figures 7Cd and 7Ee
 482 also show that the X line (at the N value of the X line in Figures 7Bd and 7De) has an
 483 alignment close to that of \mathbf{e}_M .

484 At later times starting at about $t = 26.2$ s, \mathbf{e}_m changes direction. This seems to
 485 occur in conjunction with a change in the direction of the magnetic field, as shown in
 486 Figure 6f. Note in particular the change in the M and L components of the magnetic
 487 field after $t = 26.7$ s. The linear reconstruction also shows that the X line, as indicated
 488 by $B_N = 0$ (white color in Figures 7C and 7E), starts to turn away from \mathbf{e}_M toward
 489 positive \mathbf{e}_L at $t = 26.31$ s and 26.45 s (Figures 7Eg and 7Eh).

490 Again, we chose to use the linear reconstruction because the model magnetic field
 491 was almost exactly the same as the observed field, and because it avoids wild variation
 492 of the field far from the spacecraft locations. But if we use the “3D Reduced Quadratic”
 493 model of Denton et al. (2020), the X line is again roughly oriented with \mathbf{e}_M when the
 494 spacecraft are closest to the X line, although the reconstructions yield some strange be-
 495 havior, like X lines for some M values, but not others, when the spacecraft are not close
 496 to the X line (not shown).

497 So in conclusion, the \mathbf{e}_m direction as determined from MDD is not necessarily reli-
 498 able, and it is not constant. But nearest to the X line, it may be close to the M direc-
 499 tion, and we do not find it more than about 20° off from the M direction (Figure 6j),
 500 except before $t = 24.3$ s, when it is most closely aligned with the L direction (Figure 6c).

501 There is only about 1.7 s difference between 24.3 s and the closest approach to the
 502 X line at about 26 s. Based on the ion velocity and the Spatio-Temporal Difference tech-
 503 nique, STD (Shi et al., 2006, 2019), the velocity of the magnetic structure relative to the
 504 spacecraft is no more than about 100 km/s, and the ion inertial length, d_i , is about 700 km.
 505 Based on this data, the X line might be oriented close to \mathbf{e}_M or $\mathbf{e}_{M'}$ only within a dis-
 506 tance much smaller than d_i for real events observed in space. But note that $t = 24.3$ s
 507 precedes the crossing of the current sheet, which starts at 24.5 s ((Figure 6f). So here,
 508 the current sheet thickness seems to be more relevant than the distance in d_i ; the min-
 509 imum gradient direction is more closely aligned with M or M' than with L within a dis-
 510 tance of about one half current sheet thickness from the center of the current sheet.

511 6 Discussion and Conclusions

512 For certain purposes, it may be useful to study magnetic reconnection using a co-
 513 ordinate system with L based on maximum variance of the magnetic field (Denton et
 514 al., 2018). But if one wants to find the best coordinate system for a 2D description, as
 515 for instance would be used in a 2D simulation, the optimal coordinate system would use
 516 M' in the direction of zero gradient. For anti-symmetric reconnection in the magneto-
 517 tail, with zero guide field, this is not an issue in principle (although for the 11 July 2017
 518 magnetotail reconnection event, it was problematic finding \mathbf{e}_L from MVA (Genestreti
 519 et al., 2018)). For anti-symmetric reconnection, the invariant direction should be orthog-
 520 onal to the direction of maximum variance. But for asymmetric reconnection, with a dif-
 521 ferent magnetic field on either side of the current sheet, results by Liu et al. (2018) sug-

gest that the orientation of the X line will be roughly along the bisection of the directions of the magnetic field on the two sides of the current sheet. In the case of Liu et al.’s simulation of magnetopause reconnection studied here, we showed that the orientation of the X line counterclockwise from y was $\theta_{\text{Xline}} = -14.6^\circ$ (Figures 1Aa and 1Ab), very close to the value -14.9° that results from bisection of the directions of the magnetic field in the initial magnetosphere and magnetosheath.

6.1 How can we determine the orientation of the X line from spacecraft data?

Based on Figure 1, the orientation of the X line can be determined at distances from the X line of the order of the current sheet thickness from the MDD minimum gradient direction if that direction can be measured accurately. Unfortunately, the conditions for which the MDD minimum gradient direction can be reliably determined from spacecraft data are very restrictive (section 3.2). We showed in section 5 examples of MMS data, including one event for which the MDD minimum gradient direction could be well determined (Figures 4c), and also discussed problems determining the minimum gradient direction for the event of Pathak et al. (2022).

Our attempts to determine the X line orientation in the simulation using the maximum variance direction from MVA or MGA or using other data, such as the electron velocity, were unsuccessful (Appendix A). Based on results by Liu et al. (2018), we might be able to find at least an approximation of the X line orientation from bisection of the asymptotic magnetic field directions on the magnetosphere and magnetosheath sides of the current sheet. We found (Appendix C) that for intervals of plus or minus about $3 d_i$ around the maximum magnetic field gradient (about two times the current sheet thickness, $1.6 d_i$), the direction of the bisected magnetic field unit vectors was within 3° of the X line direction.

However, in order to calculate the bisection angle, the spacecraft have to sample the asymptotic field on both sides of the current sheet, and those fields must be relatively constant over the entire time of the current sheet crossing. Because of these conditions, any calculation of the X line direction based on bisection must be cautiously interpreted. For instance, constancy of solar wind conditions could be checked to see if there is evidence for stability of the X line orientation.

We used bisection to estimate the orientation of the X line for the Chen et al. (2017) event discussed in section 5.1, for which we were fairly confident that \mathbf{e}_M from MDD represented the X line orientation pretty well. Time averages of the magnetic field on either side of the current sheet were used, constraining those directions to be perpendicular to the normal direction from MDD. In that case, bisection led to an estimate of the X line orientation that was 40° off from our estimate based on MDD. But in that case, the magnetic field on both sides of the current sheet was far from steady, and plots of solar wind quantities from OmniWeb (King & Papitashvili, 2005) showed that there were dramatic changes in the solar wind quantities corresponding to the time surrounding the current sheet crossing (not shown). So in that case the estimate from bisection was probably not valid.

We were not able to use bisection for the Pathak et al. (2022) event because the spacecraft did not sample the asymptotic magnetic field on both sides of the current sheet.

Genestreti et al. (2022) compared the direction from bisection of the asymptotic magnetic field vectors and the M direction defined from $\mathbf{e}_N \times \mathbf{e}_L$ using the maximum gradient and maximum variance directions, respectively, for 22 reconnection events. (For a few of the events, maximum variance of the electric field was used to determine the N direction.) For most events, the angle between the bisection direction and the M direction as defined in this paper, $\theta_{\text{bisection}}$, was less than 10° (Figure 8).

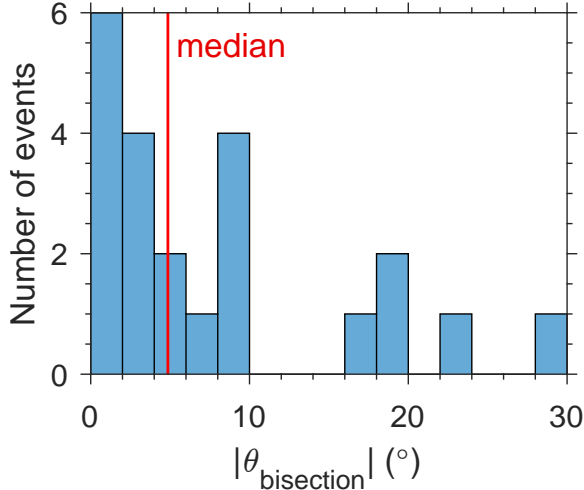


Figure 8. Histogram of angles between the direction of bisection, $\theta_{\text{bisection}}$, and the M direction (as defined in this paper), using data from Genestreti et al. (2022) (see their Figure 4a).

572 The median angle was 4.8° . Despite the precautions of Genestreti et al. (2022), there
 573 may still be some time variation of the fields, so the median value of 4.8° is probably an
 574 upper bound. So this comparison suggests that, although the bisection direction can be
 575 very different from \mathbf{e}_M , as was the case for the Chen et al. (2017) event, the difference
 576 is often not large. Taking the bisection direction as an estimate of \mathbf{e}'_M , this suggests that
 577 the difference between \mathbf{e}_M and \mathbf{e}'_M may often, but not always, be small.

578 6.2 Why did Pathak et al. (2022) get a different result for the $\mathbf{e}_{M'}$ di- 579 rection?

580 First of all, we think that it is important to use the vector magnetic field to deter-
 581 mine the minimum directional derivative. Using the local MDD coordinates, the eigen-
 582 value of the minimum directional derivative is

$$\lambda_m^2 = \frac{\partial \mathbf{B}}{\partial m} \cdot \frac{\partial \mathbf{B}}{\partial m} = \frac{\partial B_L^2}{\partial m} + \frac{\partial B_M^2}{\partial m} + \frac{\partial B_N^2}{\partial m}, \quad (1)$$

583 where, as indicated by the form with the vector \mathbf{B} , the same result would be calculated
 584 substituting other coordinates for L , M , and N shown here. Thus the minimum direc-
 585 tional eigenvalue calculated in this way takes account of the spatial derivative of all com-
 586 ponents. Furthermore, at one moment in time, the gradient of a scalar is a vector in a
 587 particular direction, so that the spatial derivative would be zero for any direction per-
 588 pendicular to that gradient.

589 If we are interpreting it correctly, Figure 4 of Pathak et al. (2022), does use the vec-
 590 tor magnetic field. But it appears to show a broad band with the minimum directional
 591 derivative in their M' direction not very different from that in their M direction. This
 592 may be because the M' direction is not well determined.

593 An extremely valuable feature of MDD is that using the gradient of the vector mag-
 594 netic field, it is possible to get time-dependent eigenvectors. As we discussed in section 5.2,
 595 it is problematic measuring the directional derivative for Pathak et al.'s event. But, ig-
 596 noring those problems, our Figure 6 shows that the minimum directional derivative is
 597 quite time-dependent, pointing mostly in our L direction near $t = 23$ s, but mostly in
 598 our M direction later. Note that Pathak et al. (2022) used a time interval from $t = 23$ s

599 to 28 s, during which we saw large time variation. Our results, here and elsewhere (Denton
600 et al., 2020) imply that there can be structural changes on the timescale of seconds.

601 Using for $t = 23$ s to 28 s our method for getting the minimum gradient direc-
602 tion by averaging the \mathbf{M}_{MDD} matrix, as described in Appendix A, we find that the min-
603 imum gradient direction is 18° off from our L direction, but the ratio between the in-
604 termediate and minimum eigenvalues is only 1.7, much smaller than adequate to expect
605 an accurate answer. If we use the second method described in Appedix A, we get a di-
606 rection that is 33° off from our M direction, a very different result. But again, the in-
607 termediate to minimum eigenvalue ratio is small, 3.2.

608 Because measurement of the ion or electron velocity was not available for MMS4
609 for this event, owing to the failure of the MMS4 FPI instrument on 7 June 2018, the gra-
610 dient of those velocities or the current density cannot be calculated.

611 Pathak et al. (2022) show results for the minimum directional derivative of E_N over
612 $t = 23$ s to 28 s, and find a direction for M' closer to the direction of L than to that
613 of M . (Although MDD using a scalar quantity cannot yield an instantaneous minimum
614 gradient direction, as discussed above, Pathak et al. found the statistical minimum di-
615 rection over that time period. See their paper for details.)

616 Using a possible calibration error of 1 mV/m (Torbert et al., 2016), MDD using
617 the vector \mathbf{E} (MDDE) has similar problems to those using \mathbf{B} . The conditions for use of
618 MDDE are again not well satisfied; during $t = 23$ s to 28 s there are only brief moments
619 of time where the intermediate gradient eigenvalue is above $10 (1 \text{ mV/m}/d_{\text{sc}})^2$, and the
620 minimum gradient eigenvalue is often not a factor of 10 lower than the intermediate gra-
621 dient eigenvalue (Text S3 and Figure S15 in the Supplementary Information). Neverthe-
622 less, if we calculate the MDDE minimum gradient direction, we find that it is very dif-
623 ferent from that of MDD using \mathbf{B} . The MDDE minimum gradient direction is (surpris-
624 ingly) closest to our N direction from $t = 23$ s to 24.2 s (when we find that the MDDB
625 minimum gradient direction is closest to our L direction) and closest to our L direction
626 at later times (when we find that the MDDB minimum gradient direction is closest to
627 our M direction). Considering this difference from the results based on \mathbf{B} , which is usu-
628 ally considered to be the most accurately measured quantity, we are hesitant to make
629 any conclusions based on MDDE.

630 A further reason to be wary of results from MDDE is that MDDE using simula-
631 tion data was not useful for determining the X line orientation (Test S1 and Figures S1-
632 S13 in the Supplementary Information).

633 6.3 Effect of secondary reconnection on the structure

634 Figures 1c–1d showed that at most locations near the simulation current sheet, the
635 MDD minimum gradient direction, if calculated accurately, could reveal the orientation
636 of the X line from which an appropriate 2D coordinate system could be determined (nearly
637 white color in Figures 1c–1d indicating near zero values for $\theta_{\text{MDDmin},z}$ and $\theta_{\text{MDDmin},xy} -$
638 14.6°). However, Figures 1Ad, 1Bd, and 1Cd show that the minimum gradient direction
639 is considerably off from the X line orientation between about $y = 60 d_i$ and $y = 77 d_i$
640 (red and blue color for $\theta_{\text{MDDmin},xy} - (-14.6^\circ)$).

641 Figure 9 shows that a flux rope due to secondary reconnection is clearly visible in
642 the simulation current density at about $y = 88 d_i$ (nearest 2D cut). The magnetic field
643 lines passing through (gold curve) or near (green curves) that flux rope go just below
644 the peak current density at $z = 3.75 d_i$ near the X line at $y = 63 d_i$ (farthest 2D cut),
645 the same location where the MDD minimum gradient direction did not reliably indicate
646 the X line orientation. Note that Figure 1Bc shows that the orientation of the MDD min-
647 imum gradient direction is especially different from that of the X line at z values $< 3.75 d_i$,

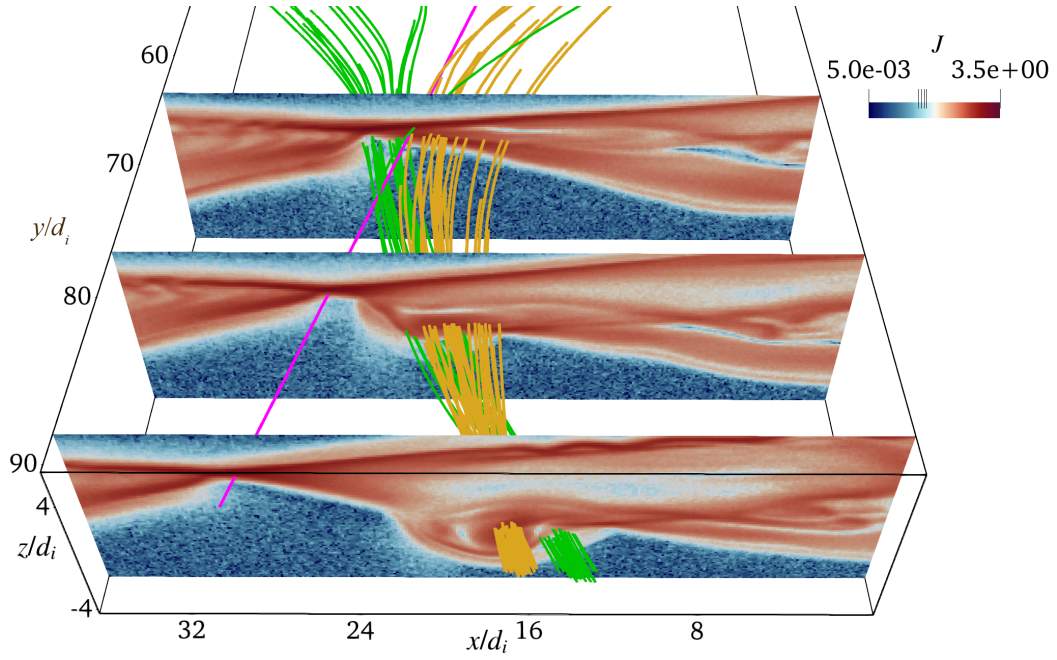


Figure 9. Magnetic field lines and 2D cuts of the simulation current density showing a flux rope due to secondary reconnection. Three 2D cuts, with color indicating the current density (on a log scale), are shown at different values of y . Two bundles of magnetic field lines are shown, one passing through the center of the flux rope at $y = 88d_i$ (gold streamlines) and the other passing just outside the flux rope (green streamlines). The diagonal purple line is the same as the dashed green line in Figure 1.

648 that is, below the current sheet. Thus it appears that this flux rope, oriented at about
 649 30 degrees away from the X line, causes the MDD minimum gradient direction to diverge
 650 from that of the primary X line.

651 The red color in Figures 1Ad and 1Bd at around $y = 70 d_i$ suggests that the in-
 652 variant direction is tilted counterclockwise from the direction of the diagonal dashed green
 653 line. To match the orientation of the flux rope in Figure 9, the angle $\theta_{\text{MDDmin},xy} - 14.6^\circ$
 654 in Figures 1Ad and 1Bd would have to be about 30° , corresponding to a tilt toward the
 655 left rather than the right in Figure 9 or Figures 1Ad. Some of the values at z below the
 656 current sheet are about 20° , but there is a lot of variation in the angle with respect to
 657 location (not shown). Therefore the minimum gradient direction from MDD may be tilted
 658 toward the flux rope orientation, but based on this data, it would be difficult to infer an
 659 accurate orientation of the large-scale X line or flux rope from just the MDD data.

660 6.4 Conclusions

661 In agreement with results by Liu et al. (2018), we found that the X line was roughly
 662 oriented for asymmetric magnetic reconnection along the bisection of the directions of
 663 the magnetic field on the two sides of the current sheet. We considered how the direc-
 664 tion of the X line could be obtained using spacecraft data. One method is to use the MDD
 665 minimum gradient direction. In the simulation, this was accurate within about 2 to 3 d_i
 666 from the X line. But results in section 5.2 suggested that MDD might not give the X
 667 line orientation outside of $0.5 d_i$ for at least one MMS event. In both cases, the relevant
 668 scale size seems to be the current sheet thickness. Certain conditions are required for the
 669 MDD minimum gradient direction to be accurately calculated from spacecraft data, as
 670 described in section 3.2. If the spacecraft cross the current sheet and sample the asymp-
 671 totic magnetic field on both sides of the current sheet, another possibility is to obtain
 672 an estimate of the X line orientation from bisection of the directions of those fields. For
 673 the simulation here, we found that an estimate accurate to about 3° could be found if
 674 the magnetic field was sampled at z values of plus or minus $3 d_i$ above the current sheet.
 675 However, such a calculation assumes that the magnetic structure and asymptotic fields
 676 are relatively constant over the time of the current sheet crossing, which will often not
 677 be the case.

678 Denton et al. (2016, 2018) previously found that the MDD minimum gradient di-
 679 rection sometimes had a significant component in the L direction if L was determined
 680 from maximum variance of the magnetic field. Results shown here in Figure 6c (at $t <$
 681 24.3 s) show that this is especially likely far away from the current sheet (see also Fig-
 682 ure 2c at locations not close to the dotted vertical line). Pathak et al. (2022) also found
 683 that the X line orientation was different from the M direction, though our results are
 684 significantly different from theirs.

685 While we agree with Pathak et al. (2022) that the X line orientation can be dif-
 686 ferent from \mathbf{e}_M determined from the cross product of the maximum gradient and max-
 687 imum variance directions, we do not agree with their statements that these results could
 688 “call for revisiting theory and simulations of guide-field magnetic reconnection” or that
 689 “many kinetic simulations may not accept a nonorthogonal X line due to a 2D system
 690 or boundary conditions.” We believe that the current methods for studying magnetic
 691 reconnection in a 2D coordinate system are still valid. Nevertheless, if one wants a 2D
 692 description of a certain event, it would be best to define the coordinate system so that
 693 the out of plane direction is M' , along the direction of the X line. Fortunately, if it is
 694 not possible to measure that direction, Figure 8 based on data from Genestreti et al. (2022)
 695 suggests that in many cases the difference in the angles may not be great.

696 The distances that we found here, MDD minimum gradient direction indicating the
 697 X line orientation within about 2 d_i of the current sheet, and bisection requiring a sam-
 698 pling of the magnetic field values about 3 d_i away from the current sheet, are of the or-

699 der of the thickness of the equilibrium current layer, $1.6 d_i$ (section 2.1). Results in sec-
 700 tion 5.2 suggest that MDD might be invalid at smaller distances from the X line in terms
 701 of d_i , but Figure 6 suggests that the times when \mathbf{e}_m is not along \mathbf{e}_M , $t < 24.4$ s (Fig-
 702 ure 6c), are when the MMS spacecraft are outside of the current sheet (region of steep
 703 variation in $B_{av,L}$ in Figure 6f). So it seems that MDD can only be used to determine
 704 the X line orientation between one half and two current sheet thicknesses away from the
 705 X line.

706 We also showed that intersection of a flux rope due to secondary reconnection with
 707 the primary X line can destroy the invariance along the X line and negate the validity
 708 of a two-dimensional description. This might occur frequently in space.

709 7 Open Research Data Availability

710 The section of data from the simulation of Liu et al. (2018) shown in Figure 1 is
 711 included in a Zenodo repository at <https://doi.org/10.5281/zenodo.7987180>. The MMS
 712 data set is available on-line at <https://lasp.colorado.edu/mms/sdc/public/links/>.

713 Acknowledgments

714 RED was supported by NASA grant 80NSSC22K1109. YL and JAA-R were supported
 715 by NASA grants 80NSSC21K2048 and 80NSSC20K1316. HH was supported by JSPS
 716 Grant-in-aid for Scientific Research KAKENHI 21K03504. We thank Neha Pathak, Ramiz
 717 Qudsi, and Tom Moore for helpful conversations and the members of the MMS Science
 718 Working Team for their contributions to the MMS data processing and to our understand-
 719 ing.

720 Appendix A MDD and MGA directions from intervals

721 In events observed by spacecraft, we get a sequence of data representing variation
 722 in the spatial domain (in addition to possibly significant independent time variation).
 723 In Figure A1 we consider quantities calculated through the X line along either x (Fig-
 724 ures A1a) or z (Figures A1b) at $y = 30 d_i$, that is, along the lower horizontal solid green
 725 line in Figure 1Aa or Figure 1Ba, respectively. Intervals of $\pm\Delta x$ or $\pm\Delta z$ are centered
 726 on the crossing of the X line, and the values in Figure A1 are plotted versus the inter-
 727 val.

728 We consider two methods to combine MDD or MGA data to get one matrix, ei-
 729 ther averaging the series of \mathbf{M}_{MDD} or \mathbf{M}_{MGA} matrices to get a single matrix for the eigen-
 730 value analysis (solid curves in Figures A1A–A1D), or averaging the gradient matrix \mathbf{M}_{gb} ,
 731 and then multiplying it with its transpose to get the \mathbf{M}_{MDD} or \mathbf{M}_{MGA} matrix (dotted
 732 curves in Figures A1A–A1D).

733 Figures A1A show the ratio of the maximum to intermediate eigenvalues from MDD
 734 (or MGA). All of the ratios plotted in Figures A1A are larger than 10, and except for
 735 the dotted curves in Figure A1Ab, all of the ratios are greater than 30. Figures A1B show
 736 the MDD maximum gradient eigenvector. This is often the best determined direction,
 737 and that is certainly true here, regardless of whether it is calculated from the average
 738 \mathbf{M}_{MDD} matrix or from the matrix found from the average gradient. This direction is al-
 739 most exactly that of z (as seen from the red curves in Figures A1B). That is what we
 740 would expect based on the equilibrium field that varies only with z . So the normal di-
 741 rection, \mathbf{e}_N , would be \mathbf{e}_z .

742 Since the initial equilibrium magnetic field has only the x component varying, the
 743 expected direction of the MGA and MVA maximum variance eigenvectors would be \mathbf{e}_x .
 744 If the MGA maximum variance direction were exactly in the x direction, the x compo-

Figure A1. MDD, MGA, and MVA maximum eigenvalue directions for intervals centered on the crossing of the X line of (a) $\Delta\mathbf{x}$ along \mathbf{x} , or (b) $\Delta\mathbf{z}$ along \mathbf{z} . In rows (A–G), we plot (A) the MDD maximum to intermediate eigenvalue ratio, $\lambda_{\text{MDD};\text{max}} = \lambda_{\text{MDD};\text{int}}$, (B) the MDD maximum gradient eigenvector, $\mathbf{e}_{\text{MDD};\text{max}}$, (C) the MGA maximum variance eigenvector, $\mathbf{e}_{\text{MGA};\text{max}}$, (D) the MGA maximum variance angle in the \mathbf{x} - \mathbf{y} plane counterclockwise from \mathbf{x} , $\theta_{\text{MGA};\text{max}}$, (E) the MVA maximum to intermediate eigenvalue ratio, $\lambda_{\text{MVA};\text{max}} = \lambda_{\text{MVA};\text{int}}$, (F) the MVA maximum variance eigenvector, $\mathbf{e}_{\text{MVA};\text{max}}$, and (G) the MVA maximum variance angle in the \mathbf{x} - \mathbf{y} plane counterclockwise from \mathbf{x} , $\theta_{\text{MVA};\text{max}}$. For (B) and (F), The solid and dotted curves use slightly different methods as described in the text.

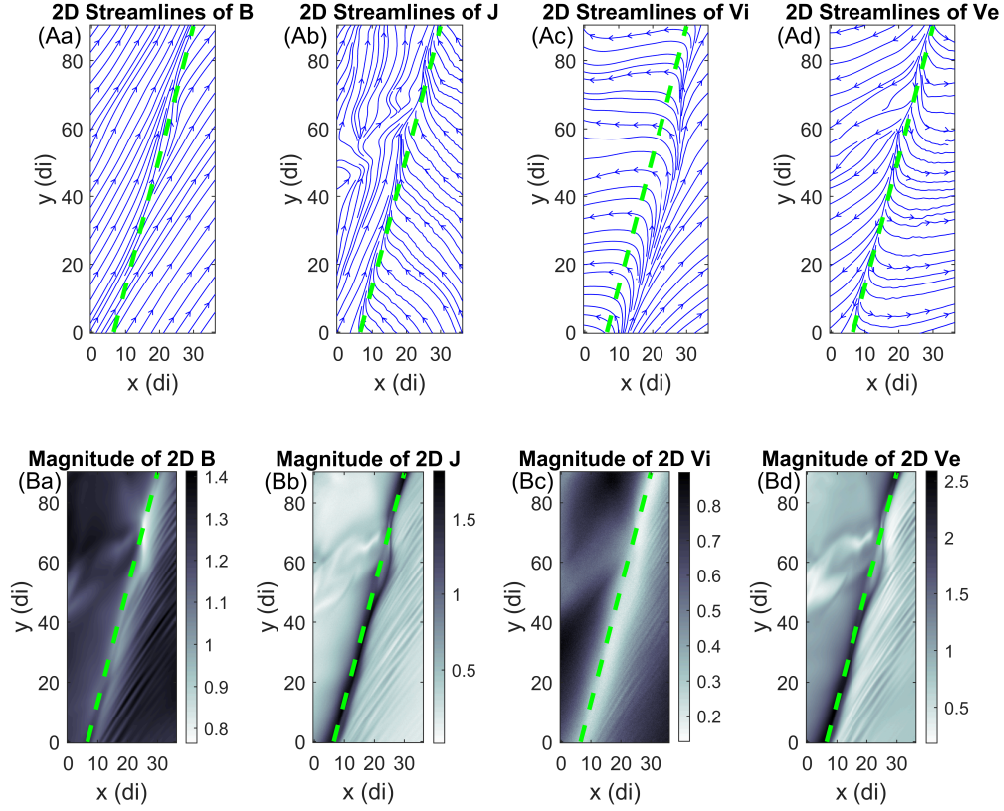


Figure A2. Streamlines and magnitude of fields in the x - y plane. 2D cuts in the x - y plane showing (A) streamlines and (B) magnitude of (a) \mathbf{B} , (b) \mathbf{J} , (c) the ion velocity V_i , and (d) the electron velocity V_e at $z = 3.75 d_i$. The fields shown are two dimensional using only the x and y components. The dashed green line is the same as that in Figure 1Aa.

Table B1. Coordinate systems for MMS events

Reference	Date	UT	Method ^a	\mathbf{e}_L (X,Y, Z) GSE	\mathbf{e}_M (X,Y, Z) GSE	\mathbf{e}_N (X,Y Z) GSE
Torbert et al. (2017)	11 Jul 2017	22:34:01.6– 22:34:02.8	MDD	(0.876,0.424, -0.230)	(-0.476,0.835, -0.275)	(0.075,0.351, 0.933)
Burch et al. (2016)	16 Oct 2015	13:07:01.6– 13:07:03.4	MVA– MDD ^b	(0.315,0.102, 0.943)	(0.534,-0.841, -0.087)	(0.785,0.531 ,-0.320)
Chen et al. (2017)	14 Dec 2015	01:17:39– 01:17:40	MDD	(0.371,-0.230, 0.899)	(-0.285,-0.950, -0.125)	(0.884,-0.209, -0.418)
Pathak et al. (2022)	27 Aug 2018	11:41:23– 11:41:28	MGA2– MDD2 ^c	(0.886,-0.398, -0.240)	(0.437,0.889, 0.139)	(0.158,-0.228, 0.961)

^aMDD calculated with average matrix, and MGA2 and MDD2 with average gradient.

^bMVA–MDD uses a combination of MVA and MDD as described in Appendix B.

^cThe digit 2 indicates the second method of calculation described in Appendix B.

794 using the method shown in the fourth column. The resulting L , M , and N coordinate
795 directions are shown in the fifth through seventh columns in GSE coordinates.

796 MDD uses the average MDD matrix (as described in section 4.2) to find \mathbf{e}_L , \mathbf{e}_M ,
797 and \mathbf{e}_N from the intermediate, minimum, and maximum gradient eigenvectors. MVA–
798 MDD uses MVA, calculated from the combination of all the MMS spacecraft magnetic
799 field measurements into a single array, for the L direction, and MDD for the N direc-
800 tion; these are combined to get a coordinate system using the hybrid method of Denton
801 et al. (2018). MGA2–MDD2 uses MGA for the L direction, and MDD for the N direc-
802 tion; the notation “2” indicates that these are calculated from the average gradient of
803 the magnetic field (the second averaging method as described in section 4.2). Then the
804 two directions are combined using the hybrid method of Denton et al. (2018).

805

References

806

- Argall, M. R., Fischer, D., Le Contel, O., Mirioni, L., Torbert, R. B., Dors, I., . . .
 Russell, C. T. (2018). The Fluxgate-Searchcoil Merged (FSM) Magnetic Field
 Data Product for MMS. *ArXiv*. doi: <https://arxiv.org/abs/1809.07388>
- Bowers, K. J., Albright, B. J., Yin, L., Daughton, W., Roytershteyn, V., Bergen, B.,
 & Kwan, T. J. T. (2009). Advances in petascale kinetic plasma simulation
 with VPIC and Roadrunner. In H. Simon (Ed.), *SCIDAC 2009: SCIENTIFIC
 DISCOVERY THROUGH ADVANCED COMPUTING* (Vol. 180). (ISSN:
 1742-6588 tex.article-number: 012055 tex.eissn: 1742-6596 tex.orcid-numbers:
 Daughton, William S/0000-0003-1051-7559 Roytershteyn, Vadim/0000-0003-
 1745-7587 Albright, Brian/0000-0002-7789-6525 Yin, Lin/0000-0002-8978-5320
 tex.researcherid-numbers: Daughton, William S/L-9661-2013 tex.unique-id:
 WOS:000281436700056) doi: [10.1088/1742-6596/180/1/012055](https://doi.org/10.1088/1742-6596/180/1/012055)
- Burch, J. L., Moore, T. E., Torbert, R. B., & Giles, B. L. (2015). Magnetospheric
 Multiscale Overview and Science Objectives. *Space Science Reviews*. doi: [10
 .1007/s11214-015-0164-9](https://doi.org/10.1007/s11214-015-0164-9)
- Burch, J. L., Torbert, R. B., Phan, T. D., Chen, L.-J., Moore, T. E., Ergun, R. E.,
 . . . Chandler, M. (2016). Electron-Scale Measurements of Magnetic Reconnec-
 tion in Space. *Science*, *110*. doi: [10.1126/science.aaf2939](https://doi.org/10.1126/science.aaf2939)
- Chen, L. J., Hesse, M., Wang, S., Gershman, D., Ergun, R. E., Burch, J., . . .
 Avanov, L. (2017). Electron diffusion region during magnetopause reconnec-
 tion with an intermediate guide field: Magnetospheric multiscale observations.
J. Geophys. Res., *122*(5), 5235–5246. doi: [10.1002/2017ja024004](https://doi.org/10.1002/2017ja024004)
- Denton, R. E., Liu, Y.-H., Hasegawa, H., Torbert, R. B., Li, W., Fuselier, S., &
 Burch, J. L. (2022, October). Polynomial reconstruction of the magnetic
 field observed by multiple spacecraft with integrated velocity determina-
 tion. *JOURNAL OF GEOPHYSICAL RESEARCH-SPACE PHYSICS*,
127(10). (tex.article-number: e2022JA030512 tex.eissn: 2169-9402 tex.orcid-numbers:
 Hasegawa, Hiroshi/0000-0002-1172-021X Burch, James/0000-0003-
 0452-8403 Fuselier, Stephen/0000-0003-4101-7901 tex.researcherid-numbers:
 MMS, Science Team NASA/J-5393-2013 Hasegawa, Hiroshi/A-1192-2007 Den-
 ton, Richard/AGE-4634-2022 tex.unique-id: WOS:000865968000001) doi:
[10.1029/2022JA030512](https://doi.org/10.1029/2022JA030512)
- Denton, R. E., Sonnerup, B. U. O., Birn, J., Teh, W. L., Drake, J. F., Swisdak,
 M., . . . Baumjohann, W. (2010). Test of methods to infer the magnetic
 reconnection geometry from spacecraft data. *J. Geophys. Res.*, *115*. doi:
[10.1029/2010ja015420](https://doi.org/10.1029/2010ja015420)
- Denton, R. E., Sonnerup, B. U. O., Hasegawa, H., Phan, T. D., Russell, C. T.,
 Strangeway, R. J., . . . Torbert, R. B. (2016). Motion of the MMS spacecraft
 relative to the magnetic reconnection structure observed on 16 October 2015 at
 1307 UT. *Geophys. Res. Lett.*, *43*(11), 5589–5596. doi: [10.1002/2016gl069214](https://doi.org/10.1002/2016gl069214)
- Denton, R. E., Sonnerup, B. U. O., Russell, C. T., Hasegawa, H., Phan, T. D.,
 Strangeway, R. J., . . . Vines, S. K. (2018). Determining L-M-N Current Sheet
 Coordinates at the Magnetopause From Magnetospheric Multiscale Data. *J.
 Geophys. Res.*, *123*(3), 2274–2295. doi: [10.1002/2017ja024619](https://doi.org/10.1002/2017ja024619)
- Denton, R. E., Torbert, R. B., Hasegawa, H., Dors, I., Genestreti, K. J., Argall,
 M. R., . . . Fischer, D. (2020, February). Polynomial reconstruction of the
 reconnection magnetic field observed by multiple spacecraft. *JOURNAL
 OF GEOPHYSICAL RESEARCH-SPACE PHYSICS*, *125*(2). (tex.article-
 number: e2019JA027481 tex.eissn: 2169-9402 tex.orcid-numbers: Hasegawa,
 Hiroshi/0000-0002-1172-021X tex.researcherid-numbers: MMS, Science
 Team NASA/J-5393-2013 Hasegawa, Hiroshi/A-1192-2007 tex.unique-id:
 ISI:000535395800016) doi: [10.1029/2019JA027481](https://doi.org/10.1029/2019JA027481)
- Fischer, D., Magnes, W., Hagen, C., Dors, I., Chutter, M. W., Needell, J., . . .
 Baumjohann, W. (2016). Optimized merging of search coil and fluxgate

859

- 860 data for MMS. *Geoscientific Instrumentation Methods and Data Systems*,
861 5(2), 521–530. doi: 10.5194/gi-5-521-2016
- 862 Fu, H. S., Cao, J. B., Vaivads, A., Khotyaintsev, Y. V., Andre, M., Dunlop, M., ...
863 Eriksson, E. (2016, February). Identifying magnetic reconnection events using
864 the FOTE method. *JOURNAL OF GEOPHYSICAL RESEARCH-SPACE*
865 *PHYSICS*, 121(2), 1263–1272. (tex.eissn: 2169-9402 tex.orcid-numbers:
866 Khotyaintsev, Yuri/0000-0001-5550-3113 Fu, Huishan/0000-0002-4701-7219
867 Vaivads, Andris/0000-0003-1654-841X Liu, Wenlong/0000-0001-7991-5067
868 dunlop, malcolm w/0000-0002-8195-5137 Liu, Wenlong/0000-0001-7991-
869 5067 tex.researcherid-numbers: Khotyaintsev, Yuri/AAX-9720-2021 Fu,
870 Huishan/E-1507-2012 Vaivads, Andris/H-8169-2013 Liu, Wenlong/Y-7669-2019
871 dunlop, malcolm w/F-1347-2010 Liu, Wenlong/G-5585-2013 tex.unique-id:
872 WOS:000373002100023) doi: 10.1002/2015JA021701
- 873 Fu, H. S., Vaivads, A., Khotyaintsev, Y. V., Olshevsky, V., Andre, M., Cao, J. B.,
874 ... Lapenta, G. (2015, May). How to find magnetic nulls and reconstruct field
875 topology with MMS data? *JOURNAL OF GEOPHYSICAL RESEARCH-*
876 *SPACE PHYSICS*, 120(5), 3758–3782. (tex.eissn: 2169-9402 tex.orcid-
877 numbers: Fu, Huishan/0000-0002-4701-7219 Khotyaintsev, Yuri/0000-0001-
878 5550-3113 Vaivads, Andris/0000-0003-1654-841X Retino, Alessandro/0000-
879 0001-5824-2852 Lapenta, Giovanni/0000-0002-3123-4024 tex.researcherid-
880 numbers: Fu, Huishan/E-1507-2012 Khotyaintsev, Yuri/AAX-9720-2021
881 Vaivads, Andris/H-8169-2013 Lapenta, Giovanni/J-5221-2016 tex.unique-id:
882 WOS:000357869600035) doi: 10.1002/2015JA021082
- 883 Fu, H. S., Wang, Z., Zong, Q., Chen, X. H., He, J. S., Vaivads, A., & Olshevsky, V.
884 (2020). Methods for finding magnetic nulls and reconstructing field topology:
885 A review. In Zong, Q and Escoubet, P and Sibeck, D and Le, G and Zhang, H
886 (Ed.), *DAYSIDE MAGNETOSPHERE INTERACTIONS* (Vol. 248, pp. 153–
887 172). (ISSN: 0065-8448 tex.orcid-numbers: Fu, Huishan/0000-0002-4701-7219
888 Zong, Qiugang/0000-0002-6414-3794 tex.researcherid-numbers: Fu, Huishan/E-
889 1507-2012 Zong, Qiugang/L-1920-2018 tex.unique-id: WOS:000637603000010)
- 890 Genestreti, K. J., Li, X., Liu, Y.-H., Burch, J. L., Torbert, R. B., Fuselier, S. A.,
891 ... Strangeway, R. J. (2022, August). On the origin of “patchy” energy
892 conversion in electron diffusion regions. *PHYSICS OF PLASMAS*, 29(8).
893 (tex.article-number: 082107 tex.eissn: 1089-7674 tex.orcid-numbers: Li,
894 Xiaocan/0000-0001-5278-8029 Genestreti, Kevin J/0000-0001-6890-2973 Giles,
895 Barbara L/0000-0001-8054-825X Nakamura, Takuma/0000-0003-4550-2947
896 Fuselier, Stephen/0000-0003-4101-7901 Burch, James/0000-0003-0452-8403
897 tex.researcherid-numbers: Li, Xiaocan/U-9696-2019 Genestreti, Kevin J/N-
898 9825-2018 Giles, Barbara L/J-7393-2017 MMS, Science Team NASA/J-5393-
899 2013 tex.unique-id: WOS:000837395400001) doi: 10.1063/5.0090275
- 900 Genestreti, K. J., Nakamura, T. K. M., Nakamura, R., Denton, R. E., Torbert,
901 R. B., Burch, J. L., ... Russell, C. T. (2018). How accurately can we measure
902 the reconnection rate E_m for the MMS diffusion region event of 11 July
903 2017? *J. Geophys. Res.*, 123(11), 9130–9149. doi: 10.1029/2018ja025711
- 904 Hesse, M., Aunai, N., Zenitani, S., Kuznetsova, M., & Birn, J. (2013, June). Aspects
905 of collisionless magnetic reconnection in asymmetric systems. *PHYSICS OF*
906 *PLASMAS*, 20(6). (tex.article-number: 061210 tex.eissn: 1089-7674 tex.orcid-
907 numbers: Zenitani, Seiji/0000-0002-0945-1815 aunai, nicolas/0000-0002-9862-
908 4318 tex.researcherid-numbers: Zenitani, Seiji/D-7988-2013 MMS, Science
909 Team NASA/J-5393-2013 Zenitani, Seiji/GQP-7514-2022 feggans, john/F-
910 5370-2012 tex.unique-id: WOS:000321273200012) doi: 10.1063/1.4811467
- 911 King, J. H., & Papitashvili, N. E. (2005). Solar wind spatial scales in and com-
912 parisons of hourly Wind and ACE plasma and magnetic field data. *J. Geophys.*
913 *Res.*, 110(A2). doi: 10.1029/2004ja010649
- 914 Le Contel, O., Leroy, P., Roux, A., Coillot, C., Alison, D., Bouabdellah, A., ... de la

- Porte, B. (2016). The Search-Coil Magnetometer for MMS. *Space Science Reviews*, 199(1-4), 257–282. doi: 10.1007/s11214-014-0096-9
- Liu, Y.-H., Hesse, M., Li, T. C., Kuznetsova, M., & Le, A. (2018, June). Orientation and stability of asymmetric magnetic reconnection X line. *JOURNAL OF GEOPHYSICAL RESEARCH-SPACE PHYSICS*, 123(6), 4908–4920. (tex.eissn: 2169-9402 tex.orcid-numbers: Li, Tak Chu/0000-0002-6367-1886 Liu, Yi-Hsin/0000-0001-5880-2645 tex.researcherid-numbers: MMS, Science Team NASA/J-5393-2013 tex.unique-id: WOS:000439803100029) doi: 10.1029/2018JA025410
- Moore, T., Fok, M., & Chandler, M. (2002, October). The dayside reconnection X line. *JOURNAL OF GEOPHYSICAL RESEARCH-SPACE PHYSICS*, 107(A10). (tex.article-number: 1332 tex.eissn: 2169-9402 tex.orcid-numbers: Fok, Mei-Ching/0000-0001-9500-866X tex.researcherid-numbers: Fok, Mei-Ching/D-1626-2012 tex.unique-id: WOS:000180353900067) doi: 10.1029/2002JA009381
- Pathak, N., Ergun, R. E., Qi, Y., Schwartz, S. J., Vo, T., Usanova, M. E., ... Nakamura, R. (2022, December). Evidence of a nonorthogonal X-line in guide-field magnetic reconnection. *ASTROPHYSICAL JOURNAL LETTERS*, 941(2). (tex.article-number: L34 tex.eissn: 2041-8213 tex.orcid-numbers: Stawarz, Julia/0000-0002-5702-5802 Vo, Tien/0000-0002-8335-1441 tex.researcherid-numbers: MMS, Science Team NASA/J-5393-2013 PATHAK, NEHA/AEF-9778-2022 Stawarz, Julia/L-7387-2016 tex.unique-id: WOS:000902413800001) doi: 10.3847/2041-8213/aca679
- Pollock, C., Moore, T., Jacques, A., Burch, J., Gliese, U., Saito, Y., ... Zeuch, M. (2016). Fast Plasma Investigation for Magnetospheric Multiscale. *Space Science Reviews*. doi: 10.1007/s11214-016-0245-4
- Qi, Y., Ergun, R., Pathak, N., Li, T. C., Eriksson, S., Chasapis, A., ... Shuster, J. (2023, June). The nonorthogonal X-line in a small guide-field reconnection event in the magnetotail. *ASTROPHYSICAL JOURNAL*, 950(2). (Number: 168 tex.eissn: 1538-4357 tex.orcid-numbers: Vo, Tien/0000-0002-8335-1441 PATHAK, NEHA/0000-0001-5567-8183 Li, Tak Chu/0000-0002-6367-1886 Eriksson, Stefan/0000-0002-5619-1577 NEWMAN, DAVID/0000-0003-0810-1204 Chasapis, Alexandros/0000-0001-8478-5797 tex.researcherid-numbers: PATHAK, NEHA/AEF-9778-2022 MMS, Science Team NASA/J-5393-2013 tex.unique-id: WOS:001012793900001) doi: 10.3847/1538-4357/acd4ba
- Qudsi, R. A., Walsh, B., Broll, J., & Haaland, S. (2022). Statistical comparison of various dayside magnetopause reconnection X-line prediction models. In *Fall meeting 2022*. (tex.organization: AGU)
- Russell, C. T., Anderson, B. J., Baumjohann, W., Bromund, K. R., Dearborn, D., Fischer, D., ... Richter, I. (2016). The Magnetospheric Multiscale Magnetometers. *Space Science Reviews*. doi: 10.1007/s11214-014-0057-3
- Shi, Q. Q., Shen, C., Dunlop, M. W., Pu, Z. Y., Zong, Q. G., Liu, Z. X., ... Balogh, A. (2006). Motion of observed structures calculated from multi-point magnetic field measurements: Application to Cluster. *Geophys. Res. Lett.*, 33(8). doi: 10.1029/2005gl025073
- Shi, Q. Q., Shen, C., Pu, Z. Y., Dunlop, M. W., Zong, Q. G., Zhang, H., ... Balogh, A. (2005). Dimensional analysis of observed structures using multipoint magnetic field measurements: Application to Cluster. *Geophys. Res. Lett.*, 32(12). doi: 10.1029/2005gl022454
- Shi, Q. Q., Tian, A. M., Bai, S. C., Hasegawa, H., Degeling, A. W., Pu, Z. Y., ... Liu, Z. Q. (2019). Dimensionality, Coordinate System and Reference Frame for Analysis of In-Situ Space Plasma and Field Data. *Space Science Reviews*, 215(4). doi: 10.1007/s11214-019-0601-2
- Sonnerup, B. U. O., & Cahill, L. J. (1967). Magnetopause Structure and Attitude from Explorer 12 Observations. *Journal of Geophysical Research*, 72(1).

- 970 Sonnerup, B. U. O., & Scheible, M. (1998). Minimum and maximum variance anal-
971 ysis. In G. Paschmann & P. Daly (Eds.), *Analysis Methods for Multi-Spacecraft*
972 *Data* (pp. 185–220). Bern Switzerland: International Space Science Institute,
973 SR-001.
- 974 Swisdak, M., & Drake, J. F. (2007). Orientation of the reconnection X-line. *Geo-*
975 *phys. Res. Lett.*, *34*(11). doi: 10.1029/2007gl029815
- 976 Torbert, R. B., Burch, J. L., Phan, T. D., Hesse, M., Argall, M. R., Shuster, J., ...
977 Saito, Y. (2018, December). Electron-scale dynamics of the diffusion region
978 during symmetric magnetic reconnection in space. *Science*, *362*(6421), 1391–+.
979 doi: 10.1126/science.aat2998
- 980 Torbert, R. B., Russell, C. T., Magnes, W., Ergun, R. E., Lindqvist, P. A., LeCon-
981 tel, O., ... Lappalainen, K. (2016, March). The FIELDS instrument suite on
982 MMS: Scientific objectives, measurements, and data products. *SPACE SCI-*
983 *ENCE REVIEWS*, *199*(1-4), 105–135. (tex.eissn: 1572-9672 tex.orcid-numbers:
984 Khotyaintsev, Yuri/0000-0001-5550-3113 Baumjohann, Wolfgang/0000-
985 0001-6271-0110 Eriksson, Anders I/0000-0003-2926-6761 Lindqvist, Per-
986 Arne/0000-0001-5617-9765 Le, Guan/0000-0002-9504-5214 Russell, Christopher
987 T/0000-0003-1639-8298 Nakamura, Rumi/0000-0002-2620-9211 LE CONTEL,
988 Olivier/0000-0003-2713-7966 Fischer, David/0000-0002-8435-7220 Plaschke,
989 Ferdinand/0000-0002-5104-6282 tex.researcherid-numbers: Khotyaintsev,
990 Yuri/AAX-9720-2021 Baumjohann, Wolfgang/A-1012-2010 Eriksson, An-
991 ders I/C-2887-2009 Lindqvist, Per-Arne/G-1221-2016 Le, Guan/C-9524-2012
992 MMS, Science Team NASA/J-5393-2013 Russell, Christopher T/E-7745-2012
993 Nakamura, Rumi/I-7712-2013 tex.unique-id: WOS:000374299800005) doi:
994 10.1007/s11214-014-0109-8